metals

MDPI

Review

A Review on the Magnetovolume Effect of the Full Heusler Alloys Ni_2MnZ (Z = In, Sn, Sb)

Takeshi Kanomata [1], Xiao Xu [2], Takuo Sakon [3,*], Yuki Nagata [3], Shin Imada [4], Toshihiro Omori [2], Ryosuke Kainuma [2], Tetsujiro Eto [5], Yoshiya Adachi [6], Takumi Kihara [7], Yasushi Amako [8], Masaaki Doi [1,9] and Yoshiya Uwatoko [10]

1 Research Institute for Engineering and Technology, Tohoku Gakuin University, Sendai 984-8588, Japan; e239982012@mail.tohoku-gakuin.ac.jp (T.K.); doi@mail.tohoku-gakuin.ac.jp (M.D.)
2 Department of Materials Science, Graduate School of Engineering, Tohoku University, Sendai 980-8579, Japan; xu@material.tohoku.ac.jp (X.X.); omori@material.tohoku.ac.jp (T.O.); kainuma@material.tohoku.ac.jp (R.K.)
3 Faculty of Advanced Science and Technology, Ryukoku University, Otsu 520-2194, Japan
4 College of Science and Engineering, Ritsumeikan University, Kusatsu 525-8577, Japan; imada@se.ritsumei.ac.jp
5 Kurume Institute of Technology, Kurume 830-0052, Japan; teto@kurume-it.ac.jp
6 Graduate School of Science and Technology, Yamagata University, Yonezawa 992-8510, Japan; adachy@yz.yamagata-u.ac.jp
7 Research Institute for Interdisciplinary Science, Okayama University, Okayama 700-8530, Japan; tkihara@s.okayama-u.ac.jp
8 Faculty of Science, Shinshu University, Matsumoto 390-8621, Japan; tenjine@shinshu-u.ac.jp
9 Faculty of Engineering, Tohoku Gakuin University, Sendai 984-8588, Japan
10 Institute for Solid State Physics, The University of Tokyo, Kashiwa 277-8581, Japan; uwatoko@issp.u-tokyo.ac.jp
* Correspondence: sakon@rins.ryukoku.ac.jp

Abstract: The full Heusler alloys Ni_2MnZ (Z = In, Sn, Sb) exhibit ferromagnetic properties with a Curie temperature (T_C) above room temperature. The magnetic properties of Ni_2MnZ (Z = In, Sn, Sb) were studied through a combination of experiments and band calculations under ambient and elevated pressures. The main results of this study open up further prospects for controlling the magnetic properties of the multifunctional Heusler alloys $Ni_2Mn_{1+x}Z_{1-x}$ (Z = In, Sn, Sb) and their practical application.

Keywords: magnetovolume effect; magnetic properties; pressure effect; itinerant electron magnets; Heusler alloys

check for updates

Received: 18 December 2024
Revised: 6 February 2025
Accepted: 10 February 2025
Published: 18 February 2025

Citation: Kanomata, T.; Xu, X.; Sakon, T.; Nagata, Y.; Imada, S.; Omori, T.; Kainuma, R.; Eto, T.; Adachi, Y.; Kihara, T.; et al. A Review on the Magnetovolume Effect of the Full Heusler Alloys Ni_2MnZ (Z = In, Sn, Sb). *Metals* **2025**, *15*, 215. https://doi.org/10.3390/met15020215

Copyright: © 2025 by the authors. Licensee MDPI, Basel, Switzerland. This article is an open access article distributed under the terms and conditions of the Creative Commons Attribution (CC BY) license (https://creativecommons.org/licenses/by/4.0/).

1. Introduction

Over the past few decades, Ni-Mn-based Heusler alloys have garnered significant interest due to their multifunctional properties. Of particular note is the extensive study of the stoichiometric shape memory alloy Ni_2MnGa, which exhibits ferromagnetic ordering below a Curie temperature (T_C) of 365 K. The shape memory effect in Ni_2MnGa is attributed to a thermoelastic martensitic transition from the cubic $L2_1$-type structure to a lower symmetry phase at approximately 200 K upon cooling [1–9]. Ni-Mn-Ga alloys with an $L2_1$-type structure exhibit a huge magnetic field-induced strain [10,11], demonstrating a faster response than other smart materials. Sutou et al. were the first to report the martensitic transition in ferromagnetic $Ni_2Mn_{1+x}Z_{1-x}$ (Z = In, Sn, Sb) Heusler alloys [12]. These alloys undergo a structural phase transition from $L2_1$ (ferromagnetic) to low-temperature phase with significantly reduced magnetization within a narrow concentration range of x [12]. Recently, Amako et al. investigated the magnetic properties of $Ni_2Mn_{1.48}Sn_{0.52}$

(x = 0.48) using the ^{119}Sn Mössbauer spectroscopy measurements [13]. Their findings revealed that the alloy was paramagnetic below the martensitic transition temperature (T_M). As the temperature was further reduced, $Ni_2Mn_{1.48}Sn_{0.52}$ regained the magnetization in its martensitic phase [13]. The Ni-Mn-Z (Z = In, Sn, Sb) Heusler alloys are highly valued for their multifunctional properties, which include significant large magnetoresistance [14,15], pronounced magnetocaloric effects [16–28], magnetic shape memory [29], exchange bias [30–32] and magnetic superelasticity [33]. The intricate interplay between these physical properties and the magnetostructural coupling between their magnetic and structural degrees of freedom is a subject of ongoing research. A pivotal element of magnetostructural transition is the magnetovolume effect.

The magnetovolume effect is defined as the interaction between magnetism and material volume changes. It is well understood that applying pressure to a ferromagnet affects its magnetization and Curie temperature. Conversely, applying a magnetic field after saturation magnetization causes volumetric changes in ferromagnets, a phenomenon known as forced volume magnetostriction. As the temperature falls below the Curie temperature, the lattice parameters deviate from the normal thermal expansion curve trajectory. Chernenko et al. documented magnetovolume effect in ferromagnetic shape memory Ni-Mn-Ga Heusler alloys, showing its significance in studying magnetostructural behaviors [34]. More recently, Eto et al. provided the experimental insights into the magnetovolume effect for stoichiometric Ni_2MnGa [35]. With the burgeoning number of studies on multifunctional materials such as $Ni_2Mn_{1+x}Z_{1-x}$ (Z = In, Sn, Sb), there has been an increase in the literature discussing the magnetovolume effect in the parent Heusler alloys Ni_2MnZ (Z = In, Sn, Sb).

The structure of this paper is organized as follows: In Section 2, the key experimental techniques are briefly described. Section 3 explores the magnetic and electronic properties of Ni_2MnZ (Z = In, Sn, Sb) at ambient pressure. Section 4 examines the magnetovolume effect, specially focusing on how pressure influences spontaneous magnetization and the Curie temperature of Ni_2MnZ (Z = In, Sn, Sb). Lastly, a list of abbreviations and symbols used in the text is provided.

2. Experimental Methodology

Ni_2MnZ (Z = In, Sn, Sb) alloys were synthesized by arc-melting or induction-melting processes of the appropriate quantities of the high purity constituent elements in an argon atmosphere. Subsequently, the reaction products were annealed at high temperatures. The crystallographic properties of Ni_2MnZ (Z = In, Sn, Sb) were investigated at room temperature by X-ray powder diffraction experiments. The static magnetic properties were measured by means of a commercial superconducting quantum interference device (SQUID) magnetometer or a magnetic balance. Some authors used an initial permeability measurement system to determine the Curie temperature of Ni_2MnZ (Z = In, Sn, Sb).

The Curie temperature under pressure was determined by an *ac* transformer method: an *ac* current flowed in the primary coil and the second voltage, which is directly proportional to initial permeability, was recorded as a function of temperature at various pressures. The pressure was generated using a piston-cylinder type apparatus. Magnetization measurements at a high pressure of Ni_2MnSn were carried out using the SQUID magnetometer (Quantum Design Co., Ltd. San Diego, CA, USA) with a miniature high-pressure clamp cell. The forced magnetostriction measurements for Ni_2MnIn and Ni_2MnSn were performed using a strain gauge method.

3. Magnetic and Electronic Properties of Ni_2MnZ (Z = In, Sn, Sb) at Ambient Pressure

The Heusler alloys Ni_2MnZ (Z = In, Sn, Sb) crystallize in a cubic $L2_1$-type structure belonging to the space group: $Fm\bar{3}m$. As illustrated in Figure 1, the $L2_1$ structure consists of four interpenetrating fcc sublattices A, B, C and D. The fractional coordinates of the $L2_1$-type structure are given in the caption of Figure 1.

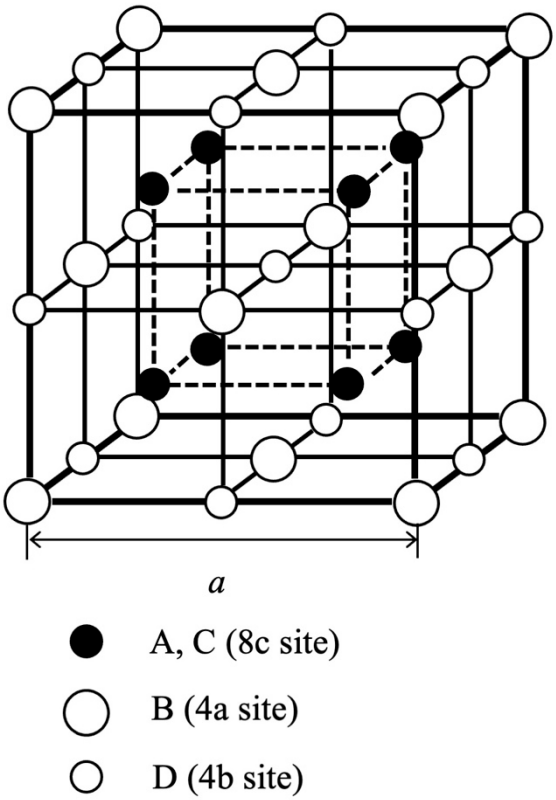

Figure 1. Crystal structure of Ni_2MnZ (Z = In, Sn, Sb) Heusler alloys. The sites are presented by A, B, C and D. A: 1/4, 1/4, 1/4; B: 0, 0, 0; C: 3/4, 3/4, 3/4; D: 1/2, 1/2, 1/2.

In the ordered Ni_2MnZ (Z = In, Sn, Sb), Ni atoms are located at the A and C sites (8c site), while Mn and Z (Z = In, Sn, or Sb) atoms occupy the B (4a) and D (4b) sites, respectively. These alloys display conventional ferromagnetic behavior, with long range Ruderman–Kittel–Kasuya–Yoshida (RKKY)-like exchange interactions mediated by conduction electrons facilitating ferromagnetic ordering [36]. The martensitic transition, often observed in Mn-rich Ni_2MnZ (Z = In, Sn, Sb) alloys, does not occur across the entire temperature spectrum in the stoichiometric compositions of Ni_2MnZ (Z = In, Sn, Sb). Various researchers have conducted extensive magnetization measurements to investigate the properties of Ni_2MnZ (Z = In, Sn, Sb) alloys. The values of T_C for Ni_2MnZ (Z = In, Sn, Sb) are detailed in Tables 1–3. The lattice parameter a of Ni_2MnZ (Z = In, Sn, Sb) at room temperature is consolidated in these tables. The sequence of lattice parameters decreases in the order of Z = In, Sn to Sb for these alloys. Variations in the experimental values of T_C for Ni_2MnZ (Z = In, Sn, Sb) were observed, which can be attributed to several factors, including preparation conditions of specimen, variations in the methodologies used for determining T_C, presence of atomic disorder and minor deviation in the stoichiometric ratios of the specimens prepared.

Table 1. The experimental values of the lattice constant a at room temperature, the Curie temperature T_C, the magnetic moment per formula unit p_s at low temperatures, the paramagnetic Curie temperature θ_p and the effective magnetic moment p_{eff} for Ni_2MnIn. Numerical data marked with * were taken analytically from the data given as figure.

a [Å]	T_C [K]	p_s [μ_B]	θ_p [K]	p_{eff} [μ_B]	References
6.069	314	4.40	319	5.14	[1]
-	228	-	-	-	[37]
6.068	323	4.40	-	-	[38]
-	323	-	-	-	[39]
6.075	-	4.34	-	-	[40]
6.074 ± 0.002	320 ± 2	4.45	-	-	[41]
-	314 ± 1	4.57 ± 0.04	-	-	[42]
6.070	315	-	350	4.69	[43]
-	350	-	-	-	[44]
6.07	308	-	-	-	[45]
6.048	-	-	-	-	[46]
6.071	290	-	-	-	[47]
6.073 *	305 *	3.83 *	-	-	[48]
6.078	315 *	4.30 *	-	-	[49]
-	-	4.5 *	-	-	[50]
-	316	-	-	-	[51]
-	316 *	4.3 *	-	-	[52]
6.060	-	-	-	-	[53]
6.0610	~315	~4.63	-	-	[54]
6.0591 ± 0.003	~314	~4.58	322	~4.96	[55]
-	314	-	-	-	[56]
6.076 ± 0.021	317	-	-	-	[57]
-	304.5 *	4.29 *	-	-	[58]
-	310	-	-	-	[59]

Table 2. The experimental values of the lattice constant a at room temperature, the Curie temperature T_C, the magnetic moment per formula unit p_s at low temperatures, the paramagnetic Curie temperature θ_p and the effective magnetic moment p_{eff} for Ni_2MnSn. Numerical data marked with * were taken analytically from the data given as figures.

a [Å]	T_C [K]	p_s [μ_B]	θ_p [K]	p_{eff} [μ_B]	References
6.053	344	4.20	356	5.07	[1]
-	200	-	-	-	[37]
6.052	344	4.05	-	-	[38]
-	344	-	-	-	[39]
6.048	345	4.01	-	-	[40]
-	346 ± 2	3.88 ± 0.04	-	-	[42]
6.048	328	-	355	5.00	[43]
-	355	-	-	-	[44]
-	340	-	-	-	[45]
6.024	-	-	-	-	[46]
6.047 *	-	4.19 *	-	-	[50]
-	337	-	-	-	[56]
-	328	4.08	-	-	[59]
6.048	410	3.3	-	-	[60]
6.032	342	3.69	-	-	[61]
6.034 ± 0.005	-	-	-	-	[62]
6.050 ± 0.005	363 ± 10	3.2 ± 0.1	-	-	[63]
6.052	344 ± 4	4.05 ± 0.07	-	-	[64]
6.062 ± 0.003	345 ± 2	4.04 ± 0.1	359 ± 2	5.05 ± 0.25	[65]

Table 2. *Cont.*

a [Å]	T_C [K]	p_s [μ_B]	θ_p [K]	p_{eff} [μ_B]	References
6.053 ± 0.005	345 ± 2	4.07 ± 0.05	--	-	[66]
-	336 *	3.25 *	--	4.55 *	[67]
-	346 ± 2	3.88 ± 0.04	--	-	[68]
-	342	-	--	-	[69]
6.054 *	342.1 *	-	356.7*	5.2 *	[70]
-	337 ± 2	-	-	-	[71]
-	350 *	3.3 *	-	-	[72]
6.034 ± 0.005	-	4.22 ± 0.10	-	-	[73]
6.052	342	3.98	363	4.90	[74]
6.048	-	4.01	-	-	[75]
-	350	4.07	-	-	[76]
6.048	362	4.24	-	5.07	[77]
6.057 ± 0.001	342 ± 2	-	-	-	[78]
-	-	5.04	-	-	[79]
-	341.3	-	-	-	[80,81]
-	338 *	-	-	-	[82]
-	341	3.98	-	-	[83]
6.046	340	-	-	-	[84]
-	340	-	-	-	[85]
6.051 *	340 *	-	-	-	[86]
6.051 *	341.7	-	-	-	[87]
-	338 *	-	-	-	[88]
-	349	4.1 *	-	-	[89]
6.051 ± 0.001	346	4.14	343	-	[90]
-	317	3.63	-	-	[91]
-	344	4.08	-	-	[92]

Table 3. The experimental values of the lattice constant a at room temperature, the Curie temperature T_C, the magnetic moment per formula unit p_s at low temperatures, the paramagnetic Curie temperature θ_p and the effective magnetic moment p_{eff} for Ni_2MnSb.

a [Å]	T_C [K]	p_s [μ_B]	θ_p [K]	p_{eff} [μ_B]	References
6.004	365	3.52	408	4.06	[1]
-	198	-	-	-	[37]
6.000	360	3.27	-	-	[38]
-	334	-	-	-	[39]
5.982	-	3.22	-	-	[40]
-	-	3.70 ± 0.04	-	-	[42]
6.027	331	-	400	4.20	[43]
-	360	-	-	-	[44]
6.03	340	-	-	-	[45]
-	410	3.6	-	-	[60]
6.00	334	4.31	-	-	[61]
6.020 ± 0.005	381 ± 5	3.9 ± 0.1	-	-	[63]
-	334	-	-	-	[69]
-	350	3.53	-	-	[83,85]
6.009	368	3.73	-	-	[93]
6.027 ± 0.001	370	-	-	-	[94]
6.0031	360	-	-	-	[95]
6.021	353	-	-	-	[96]
5.9861 ± 0.0002	~380	--	-	-	[97]
6.011 ± 0.003	-	-	-	-	[98]
6.0113	320	-	-	-	[99]
-	329	-	-	-	[100]

Figure 2 displays the magnetization curves for the Ni_2MnSn single crystal oriented along the [100] and [110] crystallographic directions at 10 K under both ambient and elevated pressures [101]. As illustrated, the magnetic isotherms of Ni_2MnSn are indicative of ferromagnetic behavior. The magnetization M of Ni_2MnSn was found to saturate at approximately 1 kOe, indicating minimal magnetic anisotropy energy in the alloy. The spontaneous magnetization values for Ni_2MnZ (Z = In, Sn, Sb) were deduced by linearly extrapolating to $H/M = 0$ of the M^2 versus H/M curves (Arrott plots). Using this method, the spontaneous magnetic moments were calculated based on the spontaneous magnetization values. Saturation magnetization, which represents the magnetization at a high magnetic field, was observed to be nearly equivalent to the spontaneous magnetization in Ni_2MnZ (Z = In, Sn, Sb); hence, both the spontaneous and saturation magnetic moments are presented as p_s in this review.

The values of p_s for Ni_2MnZ (Z = In, Sn, Sb) are consolidated in Tables 1–3. Magnetic measurements of Ni_2MnZ (Z = In, Sn, or Sb) were conducted at elevated temperatures, significantly above their respective magnetic transition temperatures, to explore the magnetic behavior in the paramagnetic state. At these temperatures, the thermal variations in the reciprocal magnetic susceptibility $1/\chi$ for Ni_2MnZ (Z = In, Sn, Sb) conform to the Curie–Weiss law, providing further insights into the magnetic properties of these alloys. These results deduced the paramagnetic Curie temperature θ_p and the effective magnetic moment p_{eff}, with the findings detailed in Tables 1–3. Tian et al. observed a Griffiths phase within the temperature range $T_C < T < T_G$ for Ni_2MnSb, where T_G represents the onset temperature of short-range ferromagnetic correlation occurring well above T_C [100].

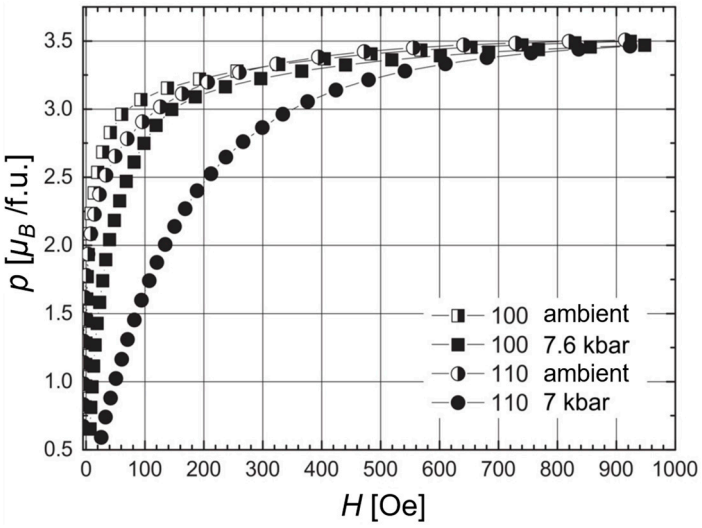

Figure 2. Magnetization curves of Ni_2MnSn single crystal oriented along [100] and [110] crystal lattice directions at 10 K under ambient and elevated pressures. This figure illustrates an increase in weak magnetic anisotropy energy of Ni_2MnSn with increasing pressure. The plots of M and H in the figure were reprinted from Ref. [101]. Copyright 2024 Copyright Taylor & Francis 's.

Numerous neutron diffraction studies have been conducted on Ni_2MnZ (Z = In, Sn, Sb) [63,79,93,102–104]. Szytuła et al. confirmed that both Ni_2MnSn and Ni_2MnSb are ferromagnetic, with Ni atoms in these alloys exhibiting zero magnetic moments [63]. Baźela-Wróbel and Szytuła performed neutron powder diffraction measurements of Ni_2MnSn at both 80 K and 293 K, concluding that the magnetic moment of Ni_2MnSn is predominantly associated with the Mn atom [104]. Noda and Ishikawa explored the magnetic interactions within Ni_2MnSn using neutron spin wave scattering, with their analysis indicating that only Mn atoms carry a magnetic moment [103]. In the 2000s, advanced techniques such as X-ray magnetic circular dichroism (XMCD) and magnetic Compton scattering experiments

were utilized to probe the electronic states of Ni_2MnZ (Z = In, Sn, Sb) [105–109]. Imada et al. investigated these properties specifically using XMCD and also discussed the electronic characteristics of these materials [105]. By applying the XMCD sum rules to the Ni and Mn $2p \rightarrow 3d$ XMCD spectra, the ratio of the magnetic moment per atom of Ni to Mn was estimated at 0.16 for Ni_2MnIn and 0.10 for Ni_2MnSn, highlighting the comparative magnetic contributions of these elements within the alloys [105]. Following this, Mund et al. conducted the magnetic Compton scattering (MCS) experiments on Ni_2MnSn, demonstrating that the Ni atoms in this alloy carry a spin moment of 0.22 μ_B at 10 K [107]. Further detailed investigations into Ni_2MnIn using XMCD were reported by Priolkar et al., who estimated the spin moments at 15 K to be approximately 3.7 μ_B/atom for Mn and about 0.34 μ_B/atom for Ni [108]. Ahuja et al., from their MCS studies on Ni_2MnIn, found the total spin moment of this alloy to be 3.86 μ_B, with the Mn contribution at 3.6 μ_B at 10 K [106]. Additionally, López-García et al. carried out neutron powder diffraction measurements on Ni_2MnIn at 50 K, reporting a magnetic moment of 0.20 μ_B for Ni atoms at this temperature [102]. These findings show the important role of Ni atoms, in conjunction with Mn, in the magnetic exchange interactions within the Ni_2MnZ (Z = In, Sn, Sb) alloys as mentioned later.

The theoretical investigations into the structural, magnetic and electronic properties of Ni_2MnZ (Z = In, Sn, Sb) have been extensively reported in the literature, focusing on band-structure and the density of states (DOS) calculations. Figure 3 presents the total DOS for both the majority and minority spins of Ni_2MnSn. In this figure, the lower-energy region below approximately 8 eV from the Fermi energy (E_F) is dominated by the Sn 5*s* states, with minor contributions from the Ni and Mn 4*s* states [110].

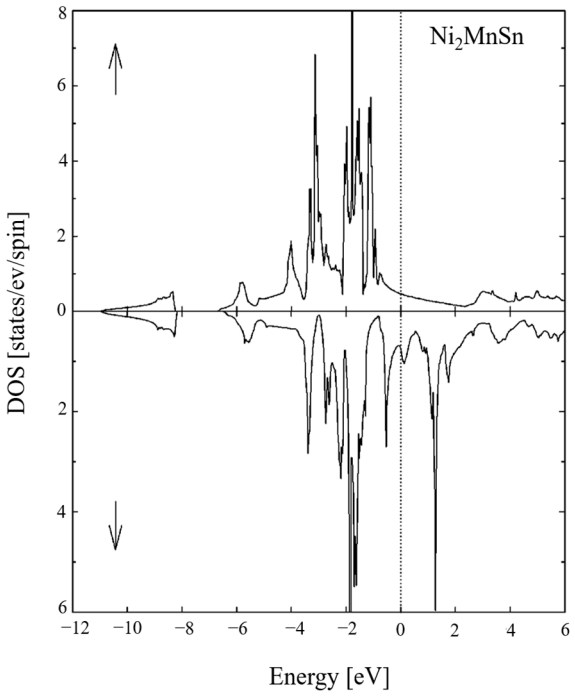

Figure 3. Total density of states (DOS) for the majority (↑) and minority (↓) states versus energy (*E*) for Ni_2MnSn. The vertical line indicates the Fermi level. The plots of DOS and *E* were reprinted by Ref. [110]. Copyright 2024 Copyright American Physical Society's.

Further details are illustrated in Figure 4, where the DOS for the *d* electron states of Ni and Mn for Ni_2MnSn are depicted. The majority (↑) spin *d* electron state densities are plotted upward, and the minority (↓) spin densities downward [110]. Specifically, the DOS for the majority-spin Mn 3*d* states are primarily found within the 0 to −6 eV range, indicating their prominence in this energy region of the valence band [110]. The Ni 3*d* states for the

majority spin are also mostly confined within the 0 to −6 eV region [110]. The overlapping of the majority spin *d* bands for Mn and Ni in Ni_2MnSn, as illustrated in Figure 4, indicates that hybridization between Mn and Ni *d* states contribute significantly to the electronic structure. Conversely, for the minority spin state, the Mn 3*d* states are positioned above the Fermi level with a peak of around 1.3 eV, while the principal contributions below the Fermi level are from the Ni 3*d* states. This distribution explains the considerable local magnetic moment observed in the Mn atoms of Ni_2MnSn, a trait common across all Ni_2MnZ (Z = In, Sn, Sb) alloys. Extensive theoretical investigations have been conducted on the net magnetic moments of the constituent elements in Ni_2MnZ (Z = In, Sn, Sb) alloys. These studies have resulted in calculated magnetic moment values summarized in Tables 4–6.

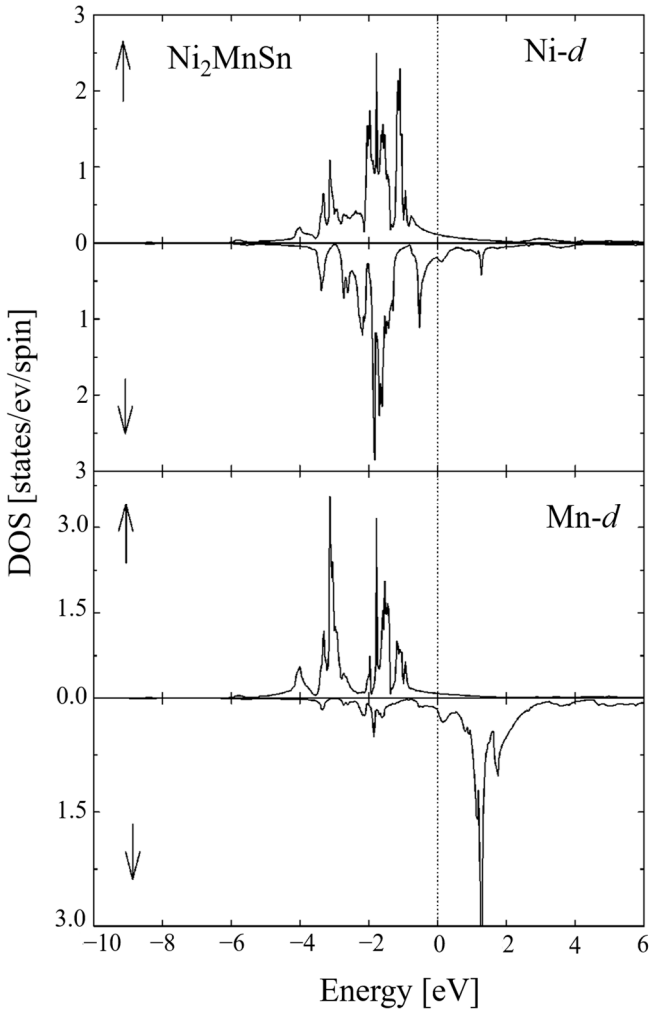

Figure 4. Majority (↑) and minority (↓) spin *d* electron state densities of Ni and Mn versus energy (*E*) for Ni_2MnSn. The vertical line indicates the Fermi level. The plots of DOS and *E* were reprinted by Ref. [110]. Copyright 2024 Copyright American Physical Society's.

Table 4. The calculated magnetic moments for Ni_2MnIn. The atomic moments of Ni, Mn and In atoms, p_{Ni}, p_{Mn} and p_{In}, are given in μ_B per atom, while the total moments, p_{tot}, are given in μ_B per formula unit. Numerical data marked with * were taken analytically from the data given as figures.

p_{tot} [μ_B]	p_{Ni} [μ_B]	p_{Mn} [μ_B]	p_{In} [μ_B]	References
4.199	0.30	3.66	−0.075	[49]
4.10	0.32	3.50	−0.04	[106]
3.91	-	3.43	-	[111]
4.16	-	-	-	[112]
4.31	-	-	-	[113]
4.208	0.277	3.719	−0.066	[114]
4.22	-	-	-	[115]
4.22	-	-	-	[116]
4.06	0.29	3.54	−0.06	[117]
4.22	0.35	3.44	−0.02	[118]
4.22	-	-	-	[119]
4.05	-	-	-	[120]
3.89	0.294	3.33	−0.0399	[121]
4.41	-	-	-	[122]
4.33	0.33	3.69	−0.08	[123,124]
4.13	0.29	3.59	-	[125]
4.44 *	-	-	-	[126]
4.205	0.354	3.579	-	[127]
3.93 *	-	-	-	[128]
4.18	0.34	3.61	−0.10	[129]
4.07	-	-	-	[130]

Table 5. The calculated magnetic moments for Ni_2MnSn. The atomic moments of Ni, Mn and Sn atoms, p_{Ni}, p_{Mn} and p_{Sn}, are given in μ_B per atom, while the total moments, p_{tot}, are given in μ_B per formula unit.

p_{tot} [μ_B]	p_{Ni} [μ_B]	p_{Mn} [μ_B]	p_{Sn} [μ_B]	References
4.08	0.25	3.62	−0.04	[90]
3.73	-	3.43	-	[111]
4.080	0.206	3.724	−0.057	[114]
4.05	-	-	-	[116]
3.93	0.22	3.55	−0.06	[117]
4.06	0.24	3.45	−0.02	[118]
3.86	-	-	-	[120]
4.035	0.252	3.588	-	[127]
3.87	-	-	-	[130]
4.10	0.024	4.01	−0.062	[131]
3.75	-	3.39	-	[132]
4.03	0.21	3.62	−0.05	[133]
4.08	0.24	3.53	−0.03	[134]
3.97	0.23	3.57	-	[135]
4.09	0.21	3.73	−0.05	[136]
3.98	0.23	3.57	−0.07	[137]
4.20	-	-	-	[138]
4.110	0.250	3.486	−0.013	[139]
4.056	-	3.539	-	[140]
4.18	0.21	3.61	-	[141]
4.07	0.16	3.84	−0.08	[142]
4.06	0.24	3.39	−0.0116	[143]
4.10	0.21	3.75	−0.06	[144]
4.09	0.26	3.53	−0.05	[145]

Table 6. The calculated magnetic moments for Ni_2MnSb. The atomic moments of Ni, Mn and Sb atoms, p_{Ni}, p_{Mn} and p_{Sb}, are given in μ_B per atom, while the total moments, p_{tot}, are given in μ_B per formula unit.

p_{tot} [μ_B]	p_{Ni} [μ_B]	p_{Mn} [μ_B]	p_{Sb} [μ_B]	References
3.39		3.13		[111]
3.950	0.143	3.696	−0.033	[114]
3.76	0.17	3.37	−0.03	[118]
3.87	-	-	-	[120]
3.72	-	-	-	[130]
4.12	-	-	-	[138]
3.998	0.158	3.553	−0.009	[139]
3.96	0.15	3.39	−0.00469	[143]
3.945	0.14	3.695	-	[146]
3.70	0.105	3.52	−0.032	[147]
3.70	-	-	-	[148]
3.90	0.16	3.60	-	[149]

The theoretical values for the magnetic moments of Ni and Mn in Ni_2MnZ (Z = In, Sn, Sb) align closely with the experimental values previously discussed. A wealth of the literature has reported on the theoretical spin resolved DOS for Ni_2MnZ (Z = In, Sn, Sb) [49,90,106,110,111,113,114,117,118,121–123,125–129,131,132,134,136,138,139,141–144,146,147,150–158]. These comprehensive studies provide detailed perspectives on the electronic interactions within these alloys, which is critical for applications exploiting their magnetic and electronic functionalities. All computational studies consistently demonstrate that the *d*-band width of Ni_2MnZ (Z = In, Sn, Sb) alloys is approximately 6 eV for Ni_2MnSn, indicating strong hybridization between the *d* states of the transition metals Ni and Mn. This hybridization extends to the *p*-states of the Z atoms, contributing to the overall electronic structure of these alloys. Crossing the Fermi level with the valence bands for both spin channels confirms their inherent metallic character. These results suggest that the *d*-electrons of Ni_2MnZ (Z = In, Sn, Sb) should be treated as itinerant electrons.

Figure 5 shows the Mn-Mn and Ni-Mn exchange interaction parameters as a function of the interatomic distance (scaled by the lattice parameter *a*) for Ni_2MnZ (Z = In, Sn, Sb) [114]. The Ni-Mn exchange interactions within these alloys are distinctly ferromagnetic and predominantly occur between nearest neighbors [114]. Notably, the strength of these inter-sublattice Ni-Mn exchange interactions varies significantly among the alloys, being particularly strong in Ni_2MnIn and decreasing markedly in Ni_2MnSn, with an even sharper decline observed in Ni_2MnSb. In Ni_2MnZ (Z = In, Sn, Sb) alloys, distinct magnetic behaviors have been observed, especially Z = Sb, in the Mn-Mn and Ni-Mn exchange interactions [114]. For Ni_2MnIn, Mn-Mn exchange interactions are positive up to the fourth coordination shell, suggesting long-range ferromagnetic tendencies. In Ni_2MnSn, the magnitudes of the nearest neighbor Ni-Mn and Mn-Mn exchange interactions are notably comparative, highlighting a balanced magnetic interaction within the alloy (Figure 5). However, in Ni_2MnSb, the Mn-Mn exchange interaction dominates, being approximately 3.6 times stronger than the first neighbor Ni-Mn exchange interaction [114]. The analysis of the exchange interactions as a function of interatomic distances in these alloys have been extensively studied [114,129,130,136,147,154,156,159–163], showing that these interactions can exhibit long-range and oscillatory characteristics, particularly in Ni_2MnSn as reported by Noda and Ishikawa using neutron spin wave scattering [103,164]. To further understand the electronic structure of Ni_2MnZ (Z = In, Sn, Sb), various spectroscopic techniques have been employed, including electron spectroscopy [118,165–169], Mössbauer spectroscopy [62,64,73,80,81,170–179], nuclear magnetic resonance (NMR) [61,180–183]

and time differential perturbed angular correlation (TDPAC) [184]. Additionally, considerable research has been directed towards investigating the transport properties of Ni_2MnZ (Z = In, Sn, Sb) alloys, focusing on the impact of electron–phonon and spin-disorder scattering on electrical resistivity [39,41,42,71,78,96,154,185–187].

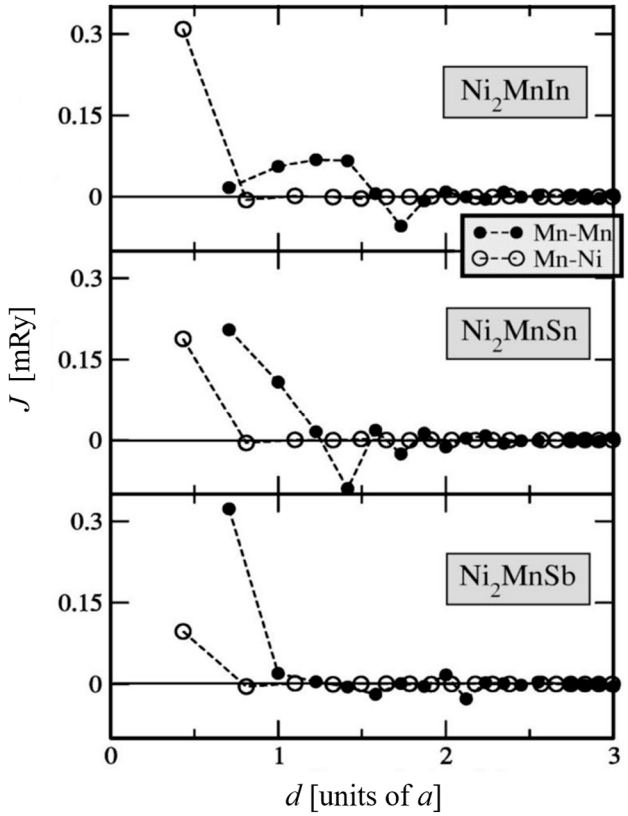

Figure 5. Parameters J of the intrasublattice Mn-Mn exchange interactions and intersublattice Ni-Mn exchange interactions as a function of the interatomic distance in Ni_2MnZ (Z = In, Sn, Sb). The distances (d) are given in the units of the lattice parameter. The plots of J and d were reprinted from Ref. [114]. Copyright 2024 Copyright American Physical Society's.

Concluding Section 3, the discussion also touches upon the issue of anti-site disorder, particularly in Ni_2MnSn, where swapping between constituent elements can lead to variations in physical properties. This disorder potentially affects both magnetic interactions and transport phenomena, presenting an additional layer of complexity in the characterization and application of these alloys. Neutron powder diffraction measurements were conducted on Ni_2MnZ (Z = Sn, Sb) alloys [63]. These studies revealed partial disorder between Ni-Mn atoms in Ni_2MnSn and between Ni-Sb atoms in Ni_2MnSb. Recently, Friák demonstrated that anti-site disorder, resulting from the swapping of constituent electrons of Ni_2MnSn, can significantly affect the magnetic properties of these materials [145,179]. Comprehensive details on how atomic disorder influences the magnetic properties of Ni_2MnSn were thoroughly discussed in the literature [145,179,188].

4. Magnetic Properties of Ni_2MnZ (Z = In, Sn, Sb) Under Pressure

Numerous studies have examined the pressure dependence of the T_C for Mn-based ferromagnetic Heusler alloys X_2MnZ (X = transition element; Z = s, p element). Notably, the impact of pressure on T_C of Ni_2MnZ (Z = In, Sn, Sb) has been extensively investigated. For all Heusler alloys, T_C consistently increased linearly with pressure up to approximately 10 kbar. Kyuji et al. [82] and Kanomata et al. [88] explored the effects of pressure on T_C of Ni_2MnSn and Ni_2MnSb by measuring the temperature dependence of initial permeability μ

under pressures ranging up to 120 kbar (and up to 100 kbar for Ni_2MnSb). High pressures were generated using a double-stage "6–8 type" multi-anvil system operated with a large hydraulic press. Figure 6 illustrates the pressure dependence of T_C for Ni_2MnSn, linearly with pressure up to 60 kbar; however, the pressure dependence of T_C shows the tendency of saturation at pressures higher than 60 kbar [88]. The value of dT_C/dp in the low-pressure region was 0.68 K/kbar, aligning closely with previously reported values (see Table 7). The pressure dependence of T_C for Ni_2MnSb was first investigated by Austin and Mishra in the 1960s [37]. They reported that the T_C of the Ni_2MnSb was independent of pressure [37]. However, subsequent studies by Kaneko et al. [69] and Kanomata et al. [43] indicated that the values of dT_C/dp at the limit of $p = 0$ for Ni_2MnSb were +3.0 and +4.0 K/kbar, respectively [43,69]. This discrepancy in values across different studies might be attributed to variations in sample disorder, as previously mentioned. The values of dT_C/dp for Ni_2MnZ (Z = In, Sn, Sb) are summarized in Table 7.

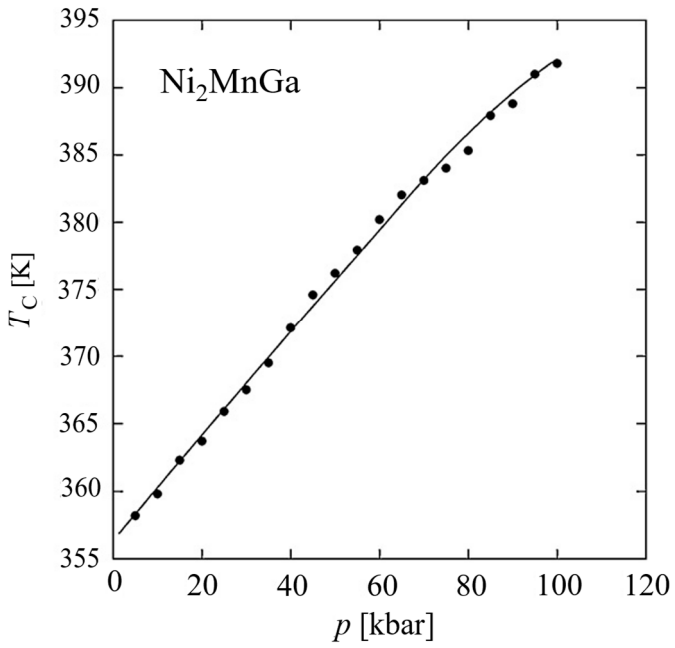

Figure 6. Curie temperature T_C versus pressure p for Ni_2MnSn. The solid line in the figure is a guide for the eye. The plots of T_C and p were reprinted from Ref. [88]. Copyright 2024 Copyright Elsevier B.V's.

Table 7. The Curie temperature T_C and the pressure derivative and coefficient of T_C, dT_C/dp and d lnTc/dp for Ni_2MnZ (Z = In, Sn, Sb). Numerical data marked with * were taken analytically from the data given as figures.

Ni_2MnIn			
T_C [K]	d T_C/dp [K/kbar]	d lnT_C/dp [kbar^{-1}]	References
228	+0.56	$+2.5 \times 10^{-3}$	[37]
315	+0.90	$+2.86 \times 10^{-3}$	[43]
314	~+0.5	$\sim+1.59 \times 10^{-3}$	[189]
Ni_2MnSn			
T_C [K]	dT_C/dp [K/kbar]	d lnT_C/dp [kbar^{-1}]	References
200	+0.62	$+3.1 \times 10^{-3}$	[37]
328	+1.40	$+4.27 \times 10^{-3}$	[43]
342	+0.55	$+1.60 \times 10^{-3}$	[69]
341.3	+0.74	$+2.18 \times 10^{-3}$	[80,81]
338 *	+0.57 *	$+1.67 \times 10^{-3}$ *	[82]

Table 7. *Cont.*

Ni_2MnSn			
T_C [K]	dT_C/dp [K/kbar]	$d\ \ln T_C/dp$ [$kbar^{-1}$]	References
341.7	+0.52	$+1.52 \times 10^{-3}$	[87]
338 *	+0.68	$+2.01 \times 10^{-3}$	[88]
317	+0.6	$+1.89 \times 10^{-3}$	[91]
Ni_2MnSb			
T_C [K]	dT_C/dp [$kbar^{-1}$]	$d\ \ln T_C/dp$ [$kbar^{-1}$]	References
198	0	0	[37]
331	+4.0	$+12.0 \times 10^{-3}$	[43]
334	+3.0	$+9.0 \times 10^{-3}$	[69]

In addition to the pressure effects on Ni_2MnZ (Z = In, Sn, Sb), other Mn-based Heusler alloys such as Au_2MnAl [190], Pd_2MnZ (Z = Sn, Sb) [37,190] and Rh_2MnZ (Z = Ge, Sn) [190] also exhibit a linear increase in T_C with increasing pressure below approximately 10 kbar. Based on these experimental findings, the dependence of the exchange interactions on Mn-Mn interatomic distances is qualitatively discussed for X_2MnZ (X = transition element; Z = *s*, *p* element) alloys. In metallic ferromagnets where Mn is the sole magnetic atom, it is well known that the Mn-Mn interatomic distances are vital parameters governing the exchange interactions between neighboring Mn atoms.

Figure 7 presents the relationship between Curie temperature and Mn-Mn interatomic distance (interaction curve) for Mn-based compounds, such as pnictides and Heusler alloys [43,60,136,191,192]. The empirical interaction curve shown in Figure 7 suggests that the pressure derivative of T_C for Ni_2MnZ (Z = In, Sn, Sb) should be positive. Indeed, as previously mentioned, the positive pressure derivatives of T_C for Ni_2MnZ (Z = In, Sn, Sb) were observed. Khovaylo et al. analyzed discussed the Mn-Mn exchange interaction curve in Ni_2MnIn-based Heusler alloys [193]. Earlier, Forrer studied the relationship between exchange interaction parameters and the nearest neighbor Mn-Mn distance across a wide range of alloys and compounds where Mn is the only potentially magnetic atom [194]. Farrer found that, generally, when the Mn-Mn nearest neighbor distance reaches a critical value of approximately 2.83 Å, the alloys and compounds exhibit a ferromagnetic behavior [194]. Furthermore, Forrer [194] observed that the alloys and compounds exhibit antiferromagnetic behavior if the Mn-Mn separation is less than this critical value. In a related study, Seshu Bai and Rajasekharan measured the exchange interaction parameters as a function of composition in various solid solutions of the metallic ferromagnet MnSb, which has a hexagonal NiAs-type structure [195]. Their findings revealed that the exchange interaction parameters in MnSb-based compounds become positive, resulting in ferromagnetic coupling when the Mn-Mn distance is equal to or greater than 2.83 Å [195]. Yamada subsequently investigated the atomic magnetic moments and exchange interactions between Mn atoms in intermetallic compounds within the Mn-Ge system [196]. The study revealed that the exchange interaction parameter was negative for Mn-Mn distances shorter than 2.9 Å and positive for larger distances [196]. In a pioneering theoretical study, Şaşıoğlu et al. examined the pressure dependence of electronic properties, exchange interactions and the T_C for Ni_2MnSn using density-functional theory [136]. Their calculation of exchange interaction parameters was based on the frozen magnon approach, while T_C under pressure was determined using the mean-field approximation. Figure 8 illustrates the pressure dependence of the first four nearest neighbor Mn-Mn exchange interaction parameters and two Ni-Mn exchange interaction parameters for Ni_2MnSn, as calculated by Şaşıoğlu et al. [136]. The results indicate that the first, second and third Mn-Mn exchange interaction parameters increase with pressure in the low-pressure range. Notably, the second and third nearest neighbor interactions increase monotonically with increasing pressure,

which primarily drives the increase in the Curie temperature [136]. The increase in Mn-Mn exchange interaction parameters with rising pressure of Ni_2MnSn is attributed to enhanced electron hopping [136]. As depicted in Figure 8, the Ni-Mn exchange interaction parameters remained largely unaffected by pressure below approximately 100 kbar. The positive value of dT_C/dp for Ni_2MnSn aligns with the empirical interaction curve shown in Figure 7. Şaşıoğlu extended the calculations of the pressure dependence of Ni_2MnSn to smaller Mn-Mn distances, down to 3.09 Å [136]. T_C decreased rapidly beyond a Mn-Mn distance of approximately 3.6 Å [136]. Experimental investigations on the effect of high pressure are highly desirable to further understand the Mn-Mn magnetic exchange interactions in Ni_2MnSn. Moreover, Bose et al. have reported the Mn-Mn exchange interactions under pressure in Ni_2MnSn [159,197]. Numerous studies have explored interatomic exchange interactions of Ni_2MnSn [36,130,135,154,163].

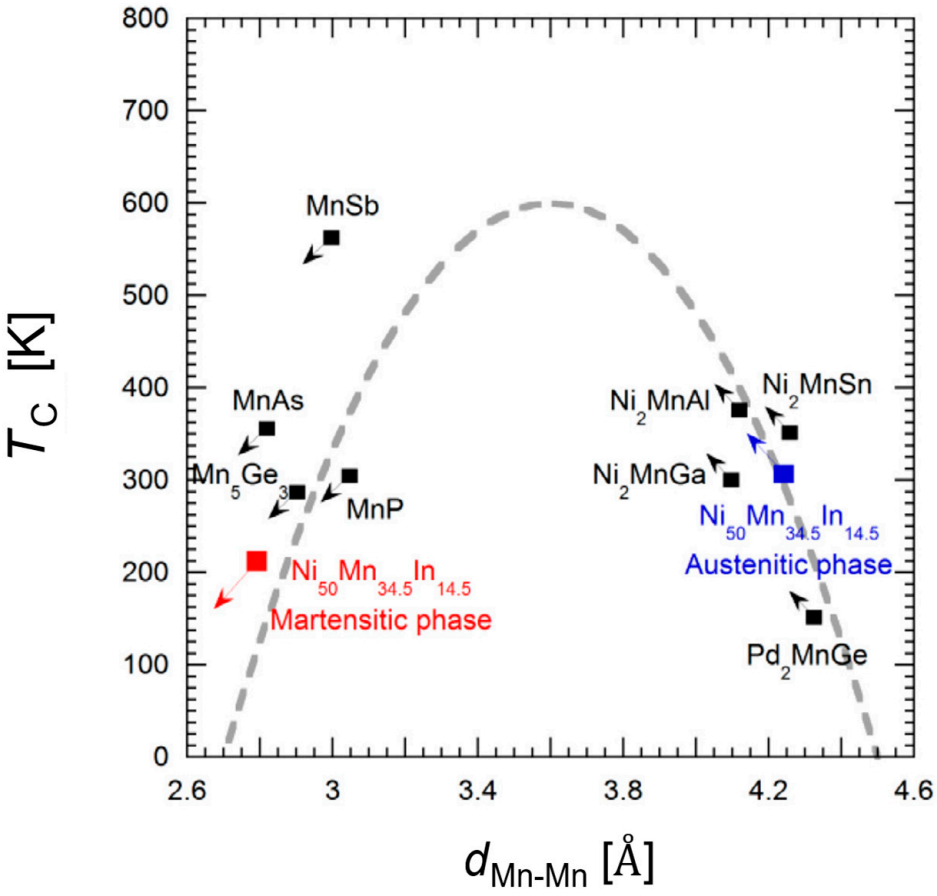

Figure 7. Curie temperature T_C versus Mn-Mn distance (d_{Mn-Mn}) curve (Castelliz-Kanomata empirical interaction curve) in various Mn-based compounds. This curve displays the dependence of T_C as a function of the nearest neighbor Mn-Mn distance for various Mn-based compounds. The arrows attached to the marks of the alloys in the figure are the symbol to show the variation in the Curie temperature T_C with increasing pressure (the upward arrow expresses the rise in T_C). The plots of T_C and d_{Mn-Mn} were reprinted from Ref. [191]. Copyright 2024 Copyright Elsevier B.V's.

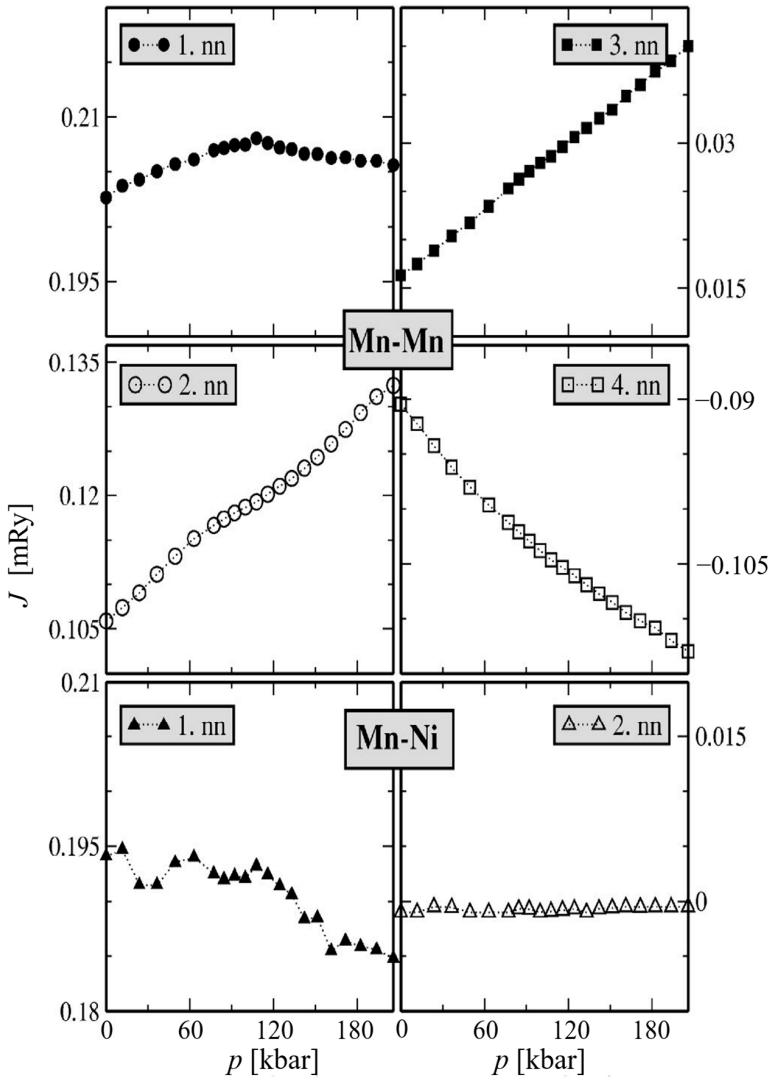

Figure 8. First four nearest neighbor Mn-Mn exchange interaction parameters and two Ni-Mn exchange interaction parameters versus pressure for Ni_2MnSn. The plots of exchange interaction parameters J and p were reprinted from Ref. [136]. Copyright 2024 Copyright American Physical Society's.

Figure 9 presents the results of theoretical calculations of the pressure dependence of magnetic moments in Ni_2MnSn [136]. As shown in Figure 9, both the total and the Mn magnetic moments decrease almost linearly with increasing pressure up to 20.6 GPa. This significant reduction in magnetic moments is attributed to band widening caused by the applied pressure. However, the behavior of Ni magnetic moment deviates noticeably from this linear trend, exhibiting oscillation, as shown in Figure 9 (for further details, refer to [136]). Hamli et al. investigated the electronic and magnetic properties of Ni_2MnSn under pressure using the generalized gradient approximation + U method [141]. Their findings similarly revealed a linear decrease in the total magnetic moment of Ni_2MnSn with increasing pressure. The positive pressure derivative of T_C for Ni_2MnSn can be explained by the competition between two opposing trends, the stronger effect of enhanced carrier hopping compared to the effect of decreasing atomic moments due to the band widening. The experimental studies of the pressure effect on the magnetic moment for Ni_2MnZ (Z = In, Sn, Sb) are fewer in number than those of the pressure effect on T_C. To our knowledge, there are no experimental data for the pressure effect of the magnetic moment in Ni_2MnZ (Z = In, Sb). The pressure effect of the magnetic moment for Ni_2MnSn was first investigated by Chieda et al. [87]. The spontaneous magnetic moment p_s at 5 K of Ni_2MnSn

decreases linearly with increasing pressure. The value of d lnp_s/dp at 5 K for Ni_2MnSn was estimated at -1.16×10^{-3} kbar^{-1} [87]. Subsequently, Kaštil et al. reported that the value of d lnp_s/dp at 5 K is -0.25×10^{-3} kbar^{-1} [91]. This value is approximately five times smaller than that reported by Chieda et al. [87]. Şaşıoğlu et al. [136] and Hamri et al. [141] calculated theoretically the pressure change in the magnetic moment (see Figure 9 for the calculation results by Şaşıoğlu et al.) for Ni_2MnSn. The values of d lnp_s/dp calculated by Şaşıoğlu et al. [136] and Hamri et al. [141] are tabulated in Table 8. Recently, Friák et al. theoretically investigated the pressure change in p_s for Ni_2MnSn using Mn-Ni, Mn-Sn and Ni-Mn swaps [145]. Their study showed that atomic disorder can strongly influence the pressure dependence of the local and total magnetic moments of Ni_2MnSn [145]. Knowledge of the elastic properties is required to understand the magnetovolume effect of Ni_2MnZ (Z = In, Sn, Sb) in more detail. Experimental data on the elastic properties of Ni_2MnZ (Z = In, Sn, Sb) are scarce. Gavriliuk et al. measured the compressibility of Ni_2MnSn using the strain gauge method under hydrostatic pressures of up to 90 kbar [80]. The experimental data were fitted to the equation of state $(V - V_0)/V_0 = -c_1p + c_2p^2$ with $c_1 = 8.64 \times 10^{-4}$ kbar^{-1} and $c_2 = 1.13 \times 10^{-6}$ kbar^{-2} [80]. The compressibility of Ni_2MnSn is comparable to that (=6.8×10^{-4} kbar^{-1}) measured at room temperature for Ni_2MnGa [35]. The elastic constants for Ni_2MnZ (Z = In, Sn, Sb) have been calculated by several authors [113,120–125,139,141–143,156,198–202]. The intriguing properties of itinerant electron magnets have been elucidated using the self-consistent renormalization spin fluctuation theory formulated by Moriya and Kawabata [203,204]. Subsequently, Takahashi advanced the novel spin fluctuation theory [205,206] in which zero-point spin fluctuation (quantum spin fluctuation) is also considered in addition to thermal spin fluctuation. Takahashi's spin fluctuation theory assumes that the total amplitude of the local spin fluctuation, which is composed of the thermal and the zero-point spin fluctuation, is constant as a function of temperatures. This postulate aligns with observations from inelastic neutron diffraction measurements on the itinerant electron magnet MnSi [207], showing minimal spin amplitude temperature dependency.

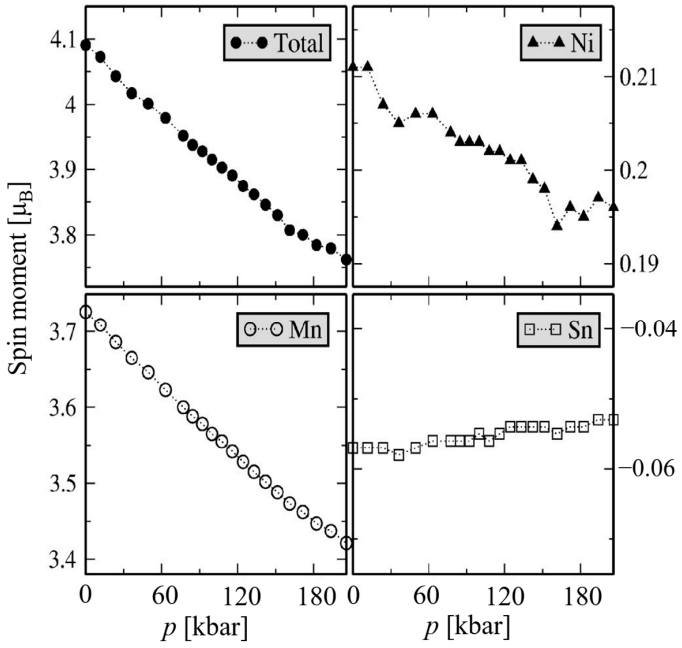

Figure 9. Total, Ni, Mn and Sn magnetic moments versus pressure for Ni_2MnSn. The plots of magnetic moments and pressure were reprinted from Ref. [136]. Copyright 2024 Copyright American Physical Society's.

Table 8. The magnetic moment per formula unit (p_s) and pressure coefficient pf p_s ($d\ln p_s/dp$) for Ni_2MnSn. Numerical data marked with * were taken analytically from the data given as figures.

	p_s [μ_B/f.u.]	d lnp_s/dp [kbar^{-1}]	References
Exp.	4.18 * (T = 5 K, p = 0.92 kbar)	-1.16×10^{-3}	[87]
Exp.	3.63 (T = 5 K, p = 0 kbar)	-0.25×10^{-3}	[91]
Calc.	4.09 (T = 0 K, p = 0 kbar))	-0.43×10^{-3} *	[136]
Calc.	4.48 (T = 0 K, p = 0 kbar)	-0.21×10^{-3} *	[141]

Takahashi's framework has been effectively applied to explore the magnetic characteristics of various itinerant electron ferromagnets, including Heusler alloys Ni_2MnGa [208–211], Co_2TiGa [190], Co_2ZrAl [190], Co_2NbGa [212], Rh_2NiGe [190] and CoVSb [190]. Additionally, this theory has recently provided insights into the magnetic properties of the 3*d* transition compound CrAlGe [213] and several actinide 5*f*-electron systems, namely UGe_2, URh_2Ge_2, UCoGe and URhGa [214,215]. According to Takahashi's theory [205,206], the fourth-order expansion F_1 coefficients (the mode–mode coupling term) of the magnetic free energy and the spontaneous magnetic moment $p_s(0)$ are expressed by the equations below.

$$F_1 = \frac{4}{15}\frac{k_B T_A^2}{T_0} \tag{1}$$

$$\frac{p_s(0)^2}{4} = \frac{15T_0}{T_A}\, c \left(\frac{T_C}{T_0}\right)^{\frac{4}{3}}, c = 0.3353 \tag{2}$$

where k_B is the Boltzmann constant. The T_0 and T_A are the parameters characterized by the spectral widths of the spin fluctuation spectra in wave vector and frequency spaces, respectively. The spontaneous magnetic moment at 0 K, $p_s(0)$, is given by $p_s(0) = M_s(0)/N_0\mu_B$, where $M_s(0)$ is the spontaneous magnetization at 0 K, μ_B the Bohr magneton and N_0 the number of magnetic sites. The values of F_1 and $p_s(0)$ are obtained experimentally from the analysis of the M^2 versus H/M plots (Arrott plots). The parameter T_0 can be expressed by eliminating T_A from Equations (1) and (2).

$$\left(\frac{T_C}{T_0}\right)^{\frac{5}{6}} = \frac{p_s(0)^2}{8\sqrt{15}\, c}\sqrt{\frac{F_1}{k_B T_C}} \tag{3}$$

Sakon et al. measured the magnetization at 4.2 K of Ni_2MnIn and Ni_2MnSn under magnetic fields up to 300 kOe [56]. Using Equations (2) and (3), they estimated the parameters T_0 and T_A of both alloys. The values of T_0 and T_A obtained are 296 and 332 K for Ni_2MnIn and 286 and 432 K for Ni_2MnSn, respectively [56].

Figure 10 shows the magnetic field dependences of magnetization, M^4 versus H/M, at T_C for Ni_2MnIn (a) and Ni_2MnS (b) [56]. As seen in Figure 10, M^4 of Ni_2MnIn and Ni_2MnSn is directly proportional to H/M at T_C. Takahashi's spin fluctuation theory provides the following relation for the magnetic field dependence of magnetization at T_C [205,206].

$$\frac{H}{M} = \frac{k_B {T_A}^3}{2\left[3\pi T_c\left(2+\sqrt{5}\right)\right]^2} \cdot \frac{M^4}{{N_0}^5 {\mu_B}^6} \tag{4}$$

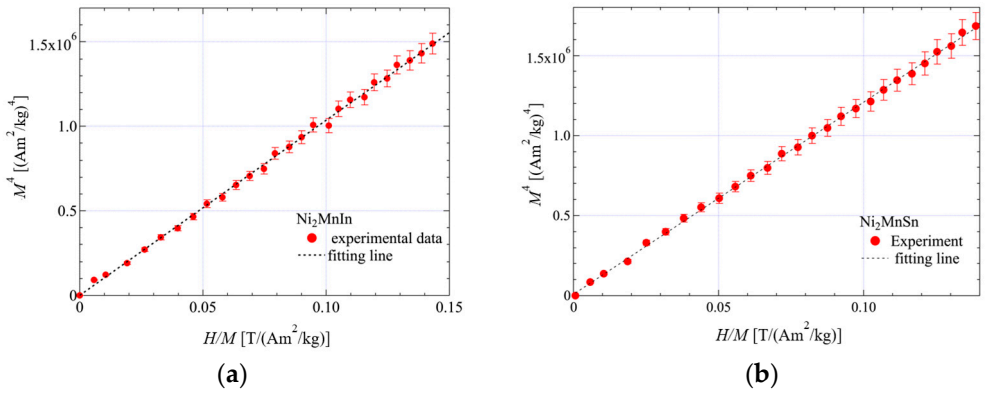

Figure 10. Magnetic field dependence of the magnetization, M^4 versus H/M, at the Curie temperature T_C for Ni_2MnIn (**a**) and Ni_2MnSn (**b**). The plots of M^4 and H/M were reprinted from Ref. [56].

Takahashi's spin fluctuation theory predicts that M^4 is proportional to H/M at $T = T_C$. As seen in Figure 10, the critical phenomena of the magnetization for Ni_2MnIn and Ni_2MnSn agree with the results predicted by Takahashi's spin fluctuation theory. From Equation (4), using their data of the M^4 versus H/M curve, Sakon et al. estimated the values of T_A for Ni_2MnIn and Ni_2MnSn [56]. The estimated values of T_A for Ni_2MnIn and Ni_2MnSn were 351 and 461 K, respectively. These values corroborate those obtained through magnetization measurements at 4.2 K.

Figure 11 shows the external magnetic field dependence of forced magnetostriction at T_C (critical forced magnetostriction) for Ni_2MnIn (a) and Ni_2MnSn (b), in which $(\Delta L/L)_{//}$ and $(\Delta L/L)_{\perp}$ are the forced linear magnetostriction parallel and perpendicular to the external magnetic field, respectively. The forced volume magnetostriction $\Delta V/V$ can be derived from the following equation,

$$\left(\frac{\Delta V}{V}\right) = \left(\frac{\Delta L}{L}\right)_{//} + 2\left(\frac{\Delta L}{L}\right)_{\perp} \quad (5)$$

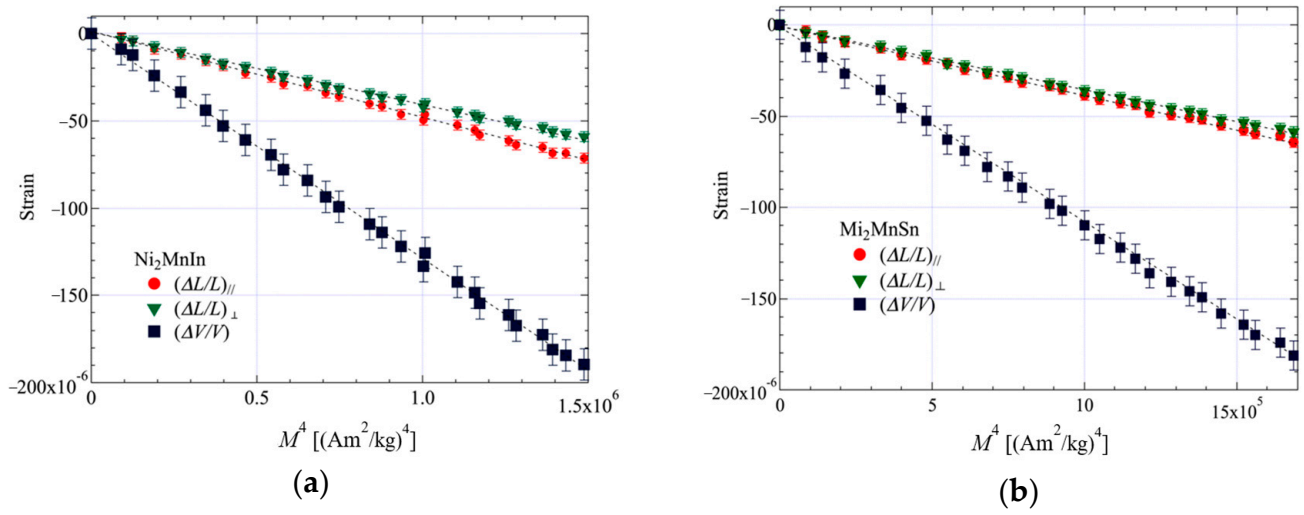

Figure 11. Forced magnetostriction versus M^4 at the Curie temperature T_C for Ni_2MnIn (**a**) and Ni_2MnSn (**b**). The plots of forced magnetostriction and M^4 were reprinted from Ref. [56].

As seen in Figure 11, the critical magnetostrictions of both alloys are proportional to M^4, and the $\Delta V/V$ versus M^4 curves of both alloys crossed the origin as indicated by the dotted linearly fitting lines. Takahashi suggested that the forced magnetostriction $\Delta V/V$ at T_C of the itinerant electron ferromagnets is proportional to the fourth power of the M;

$(\Delta V/V) \propto M^4$ [206]. The experimental observations of critical magnetostriction presented in Figure 11 for Ni_2MnIn and Ni_2MnSn align with Takahashi's spin fluctuation theory. Furthermore, recent studies of Faske et al. confirmed that the critical forced magnetostriction of $LaFe_{13-x}Si_x$ adheres to Takahashi's theory for itinerant electron ferromagnets [216].

For itinerant electron ferromagnets, the pressure dependence of $p_s(T)$ at T = 0 K, $p_s(0)$, and T_C was related by Wohlfarth as follows:

$$\frac{\mathrm{d}\ln p_s(0)}{\mathrm{d}p} = \frac{\mathrm{d}\ln T_C}{\mathrm{d}p} - \frac{5}{6}\kappa - \frac{1}{2}\frac{\mathrm{d}\ln B}{\mathrm{d}p} \tag{6}$$

$$B = \frac{1}{2\chi_0 M_s(0)^2}\left(1 + \mathrm{O}\left(T^2\right)\right) \tag{7}$$

where κ is the compressibility, χ_0 the ferromagnetic susceptibility at 0 K and $M_s(0)$ the saturation magnetization at 0 K [217]. The last two terms on the right side of Equation (6) are generally small [217]. Therefore, the relationship between d ln$p_s(0)$/dp and d lnT_C/dp can be approximated as follows:

$$\frac{\mathrm{d}\ln T_C}{\mathrm{d}p} \approx \frac{\mathrm{d}\ln p_s(0)}{\mathrm{d}p} \tag{8}$$

Equations (6) and (7) were initially derived using the molecular field theory within the framework of the itinerant electron model. Despite this, the expected linearity between d lnT_C/dp and d ln$p_s(0)$/dp often does not manifest in itinerant electron ferromagnets [190]. According to Takahashi's spin fluctuation theory, the relation between d lnT_C/dp and d ln$p_s(0)$/dp in itinerant electron ferromagnets is expressed as follows [206]:

$$\frac{\mathrm{d}\ln T_C}{\mathrm{d}p} - \frac{3}{2}\frac{\mathrm{d}\ln p_s(0)}{\mathrm{d}p} = \frac{\kappa}{4}(3\gamma_A + \gamma_0) \equiv \kappa\gamma_{0,A} \tag{9}$$

$$\kappa\gamma_A = \frac{\mathrm{d}\ln T_A}{\mathrm{d}p} \tag{10}$$

$$\kappa\gamma_0 = \frac{\mathrm{d}\ln T_0}{\mathrm{d}p} \tag{11}$$

Here, the magnetic Grüneisen parameters γ_A and γ_0 characterize the volume dependence of the spectral parameters T_A and T_0, respectively. The term of $\kappa\gamma_{0,A}$ is the weighted average of γ_A and γ_0. Using the d ln T_C/dp (= +1.52 × 10^{-3} kbar^{-1}) and d ln$p_s(0)$/dp (= −1.16 × 10^{-3} kbar^{-1}) obtained for Ni_2MnSn [87], the weighted average of $\kappa\gamma_A$ and $\kappa\gamma_0$, $\kappa\gamma_{0,A}$, was estimated to be +3.26 × 10^{-3} kbar^{-1}, where the value of d ln p_s(5 K)/dp is nearly equivalent to that of d ln$p_s(0)$/dp within the experimental error. The values of d ln$p_s(0)$/dp, d lnT_C/dp and $\kappa\gamma_{0,A}$ for the 3*d* itinerant electron ferromagnets are summarized in Table 9.

Table 9. The pressure coefficients of p_s and T_C, and the weighted average of the Grüneizen parameters $\kappa\gamma_{0,A}$ for the weak itinerant ferromagnets and the Heusler alloys. Numerical data marked with * were taken analytically from the data given as figures.

	d lnp_s/dp [kbar^{-1}]	**d lnT_C/dp [kbar^{-1}]**	**$\kappa\gamma_{0,A}$ [kbar^{-1}]**	**References**
Ni_2MnSn	-1.16×10^{-3} (5 K)	$+1.52 \times 10^{-3}$	$+3.26 \times 10^{-3}$	[87]
Co_2ZrAl	-1.78×10^{-3} (4.2 K)	-2.2×10^{-3}	$+0.47 \times 10^{-3}$	[190]
Co_2VGa	~0 (5 K)	-2.18×10^{-3}	-2.18×10^{-3}	[190]
$Ni_{74.6}Al_{25.4}$	-42.4×10^{-3} * (4.2 K)	-32.7×10^{-3}	$+31.1 \times 10^{-3}$	[218]
$Ni_{75}Al_{25}$	-8.69×10^{-3} (4.2 K)	-11.6×10^{-3}	$+1.44 \times 10^{-3}$	[219]

Table 9. *Cont.*

	d lnp_s/dp [kbar^{-1}]	d lnT_C/dp [kbar^{-1}]	$\kappa\gamma_{0,A}$ [kbar^{-1}]	References
$ZrZn_{1.9}$	-44.8×10^{-3} * (4.5 K)	-46.7×10^{-3}	$+20.5 \times 10^{-3}$ *	[220]
$TiFe_{0.5}Co_{0.5}$	-13.8×10^{-3} (0 K)	-19.3×10^{-3}	$+1.4 \times 10^{-3}$	[221]
$Fe_{0.3}Co_{0.7}Si$	-16×10^{-3} (0 K)	-16×10^{-3}	$+8 \times 10^{-3}$	[222]
Fe	-0.316×10^{-3} (4.2 K)	0	$+0.47 \times 10^{-3}$	[223,224]
Ni	-0.296×10^{-3} (4.2 K)	$+0.546 \times 10^{-3}$	$+0.99 \times 10^{-3}$	[223,224]
Co_2TiSn	~0 (7.5 K)	-0.87×10^{-3}	-0.87×10^{-3}	[225]
Co_2NbGa	-0.073×10^{-3} (10 K)	-1.84×10^{-3}	-1.73×10^{-3}	[226]

As seen in Table 9, the sign of $\kappa\gamma_{0,A}$ for the half-metallic ferromagnets Co_2TiSn and Co_2VGa is negative. Notably, Co_2NbGa with the negative sign of $\kappa\gamma_{0,A}$ is a ferromagnet with a high spin polarization [226]. On the other hand, the signs of $\kappa\gamma_{0,A}$ for the weak itinerant electron ferromagnets $Ni_{74.6}Al_{25.4}$, $ZrZn_{1.9}$, $Fe_{0.3}Co_{0.7}Si$ and $TiFe_{0.5}Co_{0.5}$ are all positive. As seen in Table 9, the signs of $\kappa\gamma_{0,A}$ for pure elements Fe and Ni are also positive. There are no experimental data on the pressure change in the spontaneous magnetization at 0 K for pure element Co. It is known that the Co_2-based Heusler alloy Co_2ZrAl is the itinerant electron ferromagnet with low spin polarization at the Fermi level [190]. Thus, Ni_2MnSn with the positive sign of $\kappa\gamma_{0,A}$ belongs to the category of the ferromagnets with the low spin polarization at the Fermi level. Jezierski calculated the spin polarization at the Fermi level of Ni_2MnSn based on local density approximation, including generalized gradient approximation (GGA and GGA + U) [142]. The obtained spin polarization of Ni_2MnSn is 7% for GGA and 16% for GGA + U. Rauf et al. also reported the low spin polarization at the Fermi level for Ni_2MnSn [155]. Notably, the spin polarizations of the typical itinerant ferromagnets Fe, Co and Ni are 44%, 34% and 11%, respectively [227]. More recently, Adachi et al. suggested that the sign of $\kappa\gamma_{0,A}$ can indicate the degree of spin polarization at the Fermi level in metallic ferromagnets [226].

5. Summary

Stoichiometric alloys of the Ni_2MnZ (Z = In, Sn, Sb) crystallize in the cubic $L2_1$-type structure and maintain this structure across the entire temperature range. These alloys exhibit ferromagnetic properties with Curie temperatures that exceed room temperature. The nearest neighboring distance between Mn atoms in these alloys is approximately 4 Å and ferromagnetic ordering is facilitated by RKKY-like exchange interactions through conduction electrons. The magnetic properties, including the magnetic moment, Curie temperature, paramagnetic Curie temperature and effective magnetic moment have been the subject of extensive studies and are the focus of this report. Band calculations suggest that the *d*-electrons of Ni_2MnZ (Z = In, Sn, Sb) should be regarded as itinerant electrons. The efficacy of the spin fluctuation theory has been demonstrated in explaining the various properties of these itinerant electron magnets. Particularly, the critical behavior of magnetization and forced magnetostriction at T_C for Ni_2MnIn and Ni_2MnSn are consistent with predictions from Takahashi's spin fluctuation theory. Many authors have studied the pressure dependence of T_C for Ni_2MnZ (Z = In, Sn, Sb). The values of dT_C/dp for Ni_2MnZ (Z = In, Sn, Sb) were found to be positive. This positive trend is consistent with the empirical interaction curve, which suggests that Curie temperatures of Ni-Mn-based Heusler alloys increase as the nearest Mn-Mn interatomic distances decrease. This behavior was explained theoretically by considering the effect of increasing carrier hopping with increasing pressure. Contrastingly, the spontaneous magnetization at 5 K of Ni_2MnSn decreased linearly with increasing pressure. Based on these experimental outcomes under pressure of Ni_2MnSn, the weighted average $\kappa\gamma_{0,A}$ of the magnetic Grüneisen parameters

for Ni_2MnSn was estimated to be $+3.26 \times 10^{-3}$ kbar^{-1}. The sign of $\kappa\gamma_{0,A}$ for weak itinerant electron ferromagnets is positive, whereas it is negative for the Heusler alloys with the high spin polarization at the Fermi level, such as the half metal Co_2TiSn. Thus, it is predicted that Ni_2MnSn falls into the category of itinerant electron ferromagnets with low spin polarization at the Fermi level, akin to pure Fe and Ni. Further magnetization measurements under pressure of Ni_2MnIn and Ni_2MnSb are highly desirable to deepen the understanding of the magnetovolume effect in Ni_2MnZ (Z = In, Sn, Sb) alloys. Recently, the multifunctional properties of Ni-Mn-based magnetic shape memory alloys with the Heusler-type structure have garnered significant interest because of their potential applications as giant caloric materials and shape memory alloys. Among the giant caloric effect, the research of large elastocaloric and barocaloric effects, which utilize the phase transition phenomenon under pressure, has been actively conducted. Insights gained from studying the magnetovolume effect of Ni_2MnZ (Z = In, Sn, Sb) could significantly advance the development and research of the Ni-Mn-Z (Z = In, Sn, Sb) giant caloric alloys.

Author Contributions: Conceptualization, T.O., R.K. and Y.U.; Methodology, T.K. (Takumi Kihara), X.X., S.I., T.O., R.K., Y.A. (Yoshiya Adachi) and Y.U.; Data analyzation, T.K. (Takeshi Kanomata), X.X., T.S., Y.N., S.I., T.O., R.K., T.E., Y.A. (Yoshiya Adachi), T.K. (Takumi Kihara), Y.A. (Yasushi Amako), M.D. and Y.U.; Figure, Y.A. (Yoshiya Adachi); Writing—Original Draft Preparation, T.K. (Takeshi Kanomata), X.X. and M.D.; Writing—Review and Editing, T.K. (Takumi Kihara), X.X., T.S., Y.N., S.I., T.O., R.K., T.E., Y.A. (Yoshiya Adachi), T.K. (Takumi Kihara), Y.A. (Yasushi Amako), M.D. and Y.U.; Supervision, T.K. (Takeshi Kanomata), T.E., Y.A. (Yoshiya Adachi), T.K. (Takumi Kihara), M.D. and T.S.; Project Administration, T.K. (Takeshi Kanomata), T.O., R.K. and Y.U.; Funding Acquisition, M.D. and T.E. All authors have read and agreed to the published version of the manuscript.

Funding: This study was supported by a Grant-in-Aid for Scientific Research (B) (Grant No. 23H01452) from the Japan Society for the Promotion of Science (JSPS) of the Ministry of Education, Culture, Spots, Science and Technology, Japan. Additionally, this work was partially supported by a Grant-in-Aid for Scientific Research (C) (Grant No. 22K04677) from JSPS.

Data Availability Statement: No new data were created or analyzed in this study. Data sharing is not applicable to this article.

Conflicts of Interest: The authors declare no conflicts of interest.

Symbols and Abbreviations Used in the Text

a	lattice parameter
$d_{\text{Mn-Mn}}$	nearest neighbor Mn-Mn distance
DOS	density of state
E	energy
E_F	Fermi energy
F_1	fourth-order expansion coefficient of the magnetic free energy
H	magnetic field
J	exchange interaction parameter
k_B	Boltzmann constant
$\Delta L/L$	forced linear magnetostriction
M	magnetization
MCS	magnetic Compton scattering
M_s	spontaneous magnetization
N_0	number of magnetic sites
p	pressure
p_{tot}	total magnetic moment per formula unit
p_{Ni}	atomic moment per Ni atom
p_s	magnetic moment per formula unit
p_{eff}	effective magnetic moment

RKKY	Ruderman–Kittel–Yoshida–Kasuya
T	temperature
T_0	parameter characterized by the spectral width of the spin fluctuation spectra in wave vector space
T_A	parameter characterized by the spectral width of the spin fluctuation spectra in frequency space
T_C	Curie temperature
TDPAC	time differential perturbed angular correlation
T_G	Griffith's temperature
T_M	martensitic transition temperature
U	Coulomb energy
V	volume
V_0	volume at ambient pressure
$\Delta V/V$	forced volume magnetostriction
XMCD	X-ray magnetic circular dichroism
γ_A, γ_0	magnetic Grüneisen parameter
$\gamma_{0,A}$	weighted average of γ_A and γ_0
θ_P	paramagnetic Curie temperature
κ	compressibility
μ_B	Bohr magneton
χ	magnetic susceptibility
χ_0	ferromagnetic susceptibility

References

1. Webster, P.J.; Ziebeck, K.R.A.; Town, S.L.; Peak, M.S. Magnetic order and phase transformation in Ni_2MnGa. *Philos. Mag. B* **1984**, *49*, 295–310. [CrossRef]
2. Chen, J.H.; Chhetri, T.P.; Wrobel, N.; Bai, X.; Young, D.P.; Dubenko, I.; Talapatra, S.; Ali, N.; Stadler, S. Phase transitions in the Co-doped Heusler alloy $Ni_2Mn_{1-x}Co_xGa$. *J. Appl. Phys.* **2024**, *136*, 233901. [CrossRef]
3. Chen, J.H.; Chhetri, T.P.; Grant, A.T.; Chang, C.-K.; Young, D.P.; Dubenko, I.; Ali, N.; Stadler, S. The effect of Cu-substitution and high-pressure synthesis on phase transitions in Ni_2MnGa Heusler alloys. *J. Alloys Compd.* **2022**, *900*, 163480. [CrossRef]
4. Cejpek, P.; Proschek, P.; Straka, L.; Heczko, O. Dependence of martensite transformation temperature on magnetic field in Ni_2MnGa and $Ni_2MnGa_{0.95}In_{0.05}$ single crystals. *J. Alloys Compd.* **2022**, *908*, 164514. [CrossRef]
5. Kovaliuk, T.; Vondráčková, B.; Valenta, J.; Colman, R.H.; Klicpera, M. Evolution of magnetic and structural phase transitions in solid solutions $Ni_2MnGa_{1-x}Ge_x$. *J. Alloys Compd.* **2022**, *894*, 162441. [CrossRef]
6. Li, G.; Xu, L.; Cao, Z. A unified physical mechanism for martensitic phase transition and ductility in Ni-Mn-based ferromagnetic shape memory alloys: The case of Cu-doped Ni_2MnGa. *J. Mater. Chem. C* **2023**, *11*, 6173. [CrossRef]
7. Karunakaran, M.; Banerjee, R. *Ab-initio* study of tuning the electronic and magnetic properties of Ni_2MnGa Heusler alloy by Co and Mn compound doping. *J. Magn. Magn. Mater.* **2023**, *568*, 170419.
8. Bhattacharya, J.; Sadhukhan, P.; Sarkar, S.; Singh, V.K.; Gloskovskii, A.; Barman, S.R.; Chakrabarti, A. Bulk electronic structure of Ni_2MnGa studied by density functional theory and hard x-ray photoelectron spectroscopy. *Phys. Rev. B* **2023**, *108*, L121114. [CrossRef]
9. Heczko, O.; Rameš, M.; Kopecký, V.; Veřtát, P.; Varga, M.; Straka, L. Magnetic and transformation properties of Ni_2MnGa combinatorically substituted with 5 at.% of transition elements from Cr to Cu-Experimental insight. *J. Magn. Magn. Mater.* **2024**, *589*, 171510. [CrossRef]
10. Ullakko, K.; Huang, J.K.; Kantner, C.; O'Handley, R.C.; Kokorin, V.V. Large magnetic-field-induced strains in Ni_2MnGa single crystals. *Appl. Phys. Lett.* **1996**, *69*, 1966–1968. [CrossRef]
11. Sakon, T.; Morikawa, K.; Narumi, Y.; Hagiwara, M.; Kanomata, T.; Nojiri, H.; Adachi, Y. Magnetostriction of Heusler ferromagnetic alloy, $Ni_2MnGa_{0.88}Cu_{0.12}$, around martensitic transition temperature. *Metals* **2023**, *13*, 1185. [CrossRef]
12. Sutou, Y.; Imano, Y.; Koeda, N.; Omori, T.; Kainuma, R.; Ishida, K.; Oikawa, K. Magnetic and martensitic transformations of NiMnX (X = In, Sn, Sb) ferromagnetic shape memory alloys. *Appl. Phys. Lett.* **2004**, *85*, 4358–4360. [CrossRef]
13. Amako, Y.; Tanaka, S.; Nakashima, M.; Eto, T.; Adachi, Y.; Kanomata, T. ^{119}Sn Mössbauer and magnetization studies of the Heusler alloy $Ni_2Mn_{1.48}Sn_{0.52}$. *J. Phys. Chem. Solids* **2023**, *172*, 111101. [CrossRef]
14. Kaletina, Y.V.; Gerasimov, E.G.; Terent'ev, P.B.; Kaletin, A.Y. Martensitic transformation and the electrical and magnetic properties of $Ni_{51-x}Mn_{36+x}Sn_{13}$ ($0 \leq x \leq 4$) alloys. *Phys. Metal. Metallogr.* **2023**, *124*, 664. [CrossRef]

15. Patel, A.K.; Samatham, S.S.; Suresh, K.G. Magnetism and transport behavior of $Ni_{42}Co_8Mn_{38}Sb_{12}$: Magnetization, electrical resistivity and Hall effect measurements. *Mater. Res. Bull.* **2022**, *146*, 111577. [CrossRef]
16. Arman, M.; Shahri, F.; Gholamipour, R.; Sohrabi, S. Effect of Al doping on the magnetic, magneto-structural, and magnetocaloric properties of Ni-Mn-In Heusler alloys. *Solid State Commun.* **2025**, *396*, 115767. [CrossRef]
17. Alamri, H.R.; Hamad, M.A. Verification of the phenomenological model's validity for the conventional and inverse magnetocaloric effects in $Ni_{50}Mn_{34}In_{16}$. *J. Supercond. Novel. Magn.* **2024**, *37*, 1917. [CrossRef]
18. Emre, B.; Yuce, S.; Kavak, E.; Saritas, S.; Cicek, M.M.; Yildirim, O.; Duman, E.; Albertini, F.; Fabbrici, S. Revealing contrary contributions of the magnetic and lattice entropy to the inverse magnetocaloric effect in magnetic shape memory alloy. *J. Appl. Phys.* **2024**, *135*, 213901. [CrossRef]
19. Kavak, E.; Cicek, M.M.; Saritas, S.; Emre, B. Investigation of the effect of martensitic phase transition temperature and Curie temperature difference on magnetic and magnetocaloric properties under low magnetic field on Si-doped Ni-Mn-In Heusler alloys. *Phys. Scr.* **2024**, *99*, 095924. [CrossRef]
20. Saritaş, S.; Çiçek, M.M.; Kavak, E.; Gurpinar, K.; Yildirim, O.; Yuce, S.; Atakol, O.; Emre, B. Tuning of the magneto-caloric effects in $Ni_{43}Mn_{46}In_{11}$ magnetic shape memory alloys by substitution of boron. *J. Phys. Condens. Matter.* **2024**, *36*, 075801. [CrossRef]
21. Sharma, J.; Coelho, A.A.; Suresh, K.G.; Alam, A. Martensitic and room-temperature magnetocaloric properties of Mn-rich Mn-Ni-Sn Heusler alloys: Experiment and theory. *Phys. Rev. B* **2024**, *109*, 064418. [CrossRef]
22. Samanta, T.; Taake, C.; Bondzio, L.; Hütten, A.; Caron, L. Interplay between the reversibility of the inverse magnetocaloric effect and kinetic arrest in Ni-Co-Mn-Sn Heusler alloys. *J. Alloys Compd.* **2024**, *1002*, 175145. [CrossRef]
23. Gamzatov, A.G.; Batdalov, A.B.; Khizriev, S.K.; Aliev, A.M.; Varzaneh, A.G.; Kameli, P. High frequency dependence of the magnetocaloric effect in the $Ni_{47}Mn_{40}Sn_{13}$ alloy: Direct measurement. *J. Mater. Sci.* **2023**, *58*, 8503. [CrossRef]
24. Cheng, Y.; Luo, X.; Cao, Y.; Xu, K.; Emelyanova, S.M.; Tyutyunnik, A.P.; Dyachkova, T.V.; Marchenkov, V.V. Magneto-structural coupling induced multiple magnetic transitions and magnetocaloric effect of $Ni_{43}Mn_{46}Sn_9Ge_2$ alloy. *J. Magn. Magn. Mater.* **2022**, *563*, 169944. [CrossRef]
25. Gamzatov, A.G.; Khizriev, S.K.; Aliev, A.M. Direct and inverse magnetocaloric effect in a $Ni_{50}Mn_{35}Al_2Sn_{13}$ Heusler-alloy ribbon sample. *Phys. Metal. Metallogr.* **2022**, *123*, 392. [CrossRef]
26. Fabbrici, S.; Cugini, F.; Orlandi, F.; Amadè, N.S.; Casoli, F.; Calestani, D.; Cabassi, R.; Cavazzini, G.; Righi, L.; Solzi, M.; et al. Magnetocaloric properties at the austenitic Curie transition in Cu and Fe substituted Ni-Mn-In Heusler compounds. *J. Alloys Compd.* **2022**, *899*, 163249. [CrossRef]
27. Ghosh, S.; Sangwan, S.; Mandal, S.; Datta, S.; Kar, M.; Singh, P.; Nath, T.K. Room temperature giant magneto-caloric effect in $Ni_{45}Mn_{44}Sn_{11-x}In_x$ (x = 1,3) disordered Heusler alloy: The role of martensite transition. *J. Magn. Magn. Mater.* **2022**, *562*, 169797. [CrossRef]
28. Lekkla, P.; Jantaratana, P. Near room-temperature magnetocaloric effect of liquid phase sintered $Ni_{50}Mn_{34-x}In_{16}Cr_x$alloys. *Solid State Commun.* **2022**, *342*, 114628. [CrossRef]
29. Sarkar, S.K.; Babu, P.D.; Sharma, V.K.; Kaushik, S.D.; Goswami, S.; Manekar, M.A. Enhanced metamagnetic shape memory effect in Heusler-type $Ni_{37}Co_{11}Mn_{43}Sn_9$ polycrystalline ferromagnetic shape memory alloy. *Acta Mater.* **2024**, *276*, 120126. [CrossRef]
30. Sharma, J.; Alam, A.; Suresh, K.G. Large magnetocaloric effect and exchange bias properties in Mn-Ni-Co-Sn full Heusler alloy. *J. Alloys Compd.* **2024**, *983*, 173908. [CrossRef]
31. Tian, F.; Chang, T.; Zhao, Q.; Cuo, J.; Xian, L.; Cao, K.; Dai, Z.; Zhang, Y.; Zhou, C.; Yang, S. A room temperature exchange bias effect caused by the coexisting martensitic phase structures in $Ni_{50}Mn_{38}Sb_{12-x}Ga_x$ polycrystalline Heusler alloys. *Appl. Phys. Lett.* **2023**, *123*, 232402. [CrossRef]
32. Kamarád, J.; Kaštil, J.; Friák, M.; Turek, I.; Kubíčková, L.; Kaman, O.; Schneeweiss, O.; Arnold, Z. Magnetization and exchange-bias effect in powders of the Heusler Ni_2MnSn-based alloys. *J. Alloys Compd.* **2024**, *976*, 173157. [CrossRef]
33. Chen, Z.; Zhang, Y.; Wang, L.; Cong, D.; Sun, X. Ultra-low stress-hysteresis and huge superelasticity in NiMn-based shape memory microwire. *Appl. Phys. Lett.* **2024**, *125*, 023102. [CrossRef]
34. Chernenko, V.A.; L'vov, V.A.; Cesari, E.; Kosogor, A.; Barandiaran, J.M. Transformation Volume Effects on Shape Memory Alloys. *Metals* **2013**, *3*, 237–282. [CrossRef]
35. Eto, T.; Nakamoto, Y.; Kagayama, T.; Adachi, Y.; Kawaguchi, S.; Hirao, N.; Uwatoko, Y.; Nagasako, M.; Kanomata, T. Pressure-induced structural phase transition in the ferromagnetic Heusler alloy Ni_2MnGa. *Phys. Rev. B* **2024**, *109*, 014101. [CrossRef]
36. Şaşıoğlu, E.; Sandratskii, L.M.; Bruno, P. Role of conduction electrons in mediating exchange interactions in Mn-based Heusler alloys. *Phys. Rev. B* **2008**, *77*, 064417. [CrossRef]
37. Austin, I.G.; Mishra, P.K. The effect of pressure on the Curie temperature and resistivity of some rare-earth metals and Heusler alloys. *Phil. Mag.* **1967**, *15*, 529–538. [CrossRef]
38. Webster, P.J. Heuler alloys. *Contemp. Phys.* **1969**, *10*, 559–577. [CrossRef]
39. Schreiner, W.H.; Brandão, D.E.; Ogiba, F.; Kunzler, J.V. Electrical resistivity of Heusler alloys. *J. Phys. Chem. Solids* **1982**, *43*, 777–780. [CrossRef]

40. Buschow, K.H.J.; van Engen, P.G.; Jongebreur, R. Magneto-optical properties of metallic ferromagnetic materials. *J. Magn. Magn. Mater.* **1983**, *38*, 1–22. [CrossRef]
41. Fraga, G.L.F.; Kunzler, J.V.; Ogiba, F.; Brandão, D.E. Electrical resistivity of the Ni_2MnIn Heusler alloy. *Phys. Stat. Sol. (a)* **1984**, *83*, K187–K190. [CrossRef]
42. Hurd, C.M.; McAlister, S.P. Galvanomagnetic properties of Ni_2MnIn, Ni_2MnSn and Ni_2MnSb Heusler alloys. *J. Magn. Magn. Mater.* **1986**, *61*, 114–120. [CrossRef]
43. Kanomata, T.; Shirakawa, K.; Kaneko, T. Effect of hydrostatic pressure on the Curie temperature of the Heusler alloys Ni_2MnZ (Z=Al, Ga, In, Sn and Sb). *J. Magn. Magn. Mater.* **1987**, *65*, 76–82. [CrossRef]
44. Fraga, G.L.F.; Brandão, D.E.; Sereni, J.G. Specific heat of X_2MnSn (X = Co, Ni, Pd, Cu), X_2MnIn (X = Ni, Pd) and Ni_2MnSb Heusler compounds. *J. Magn. Magn. Mater.* **1991**, *102*, 199–207. [CrossRef]
45. Shreder, E.I.; Kirillova, M.M. Optical properties and electronic characteristics of Heusler alloys Cu_2MnZ and Ni_2MnZ (Z = Al, In, Sn, Sb). *Phys. Met. Metallogr.* **1993**, *76*, 476–480.
46. Choi, B.S. Thermal, magnetic and magnetoelastic data on three different Heusler alloys based on Ni-Mn-X (X = Ga, In, or Sn). *IEEE Trans. Mag.* **2006**, *42*, 1770–1777. [CrossRef]
47. Krenke, T.; Acet, M.; Wassermann, E.F.; Moya, X.; Mañosa, L.; Planes, A. Ferromagnetism in the austenitic and martensitic states of Ni-Mn-In alloys. *Phys. Rev. B* **2006**, *73*, 174413. [CrossRef]
48. Kanomata, T.; Yasuda, T.; Sasaki, S.; Nishihara, H.; Kainuma, R.; Ito, W.; Oikawa, K.; Ishida, K.; Neumann, K.-U.; Ziebeck, K.R.A. Magnetic properties on shape memory alloys $Ni_2Mn_{1+x}In_{1-x}$. *J. Magn. Magn. Mater.* **2009**, *321*, 773–776. [CrossRef]
49. Chatterjee, S.; Singh, V.R.; Deb, A.K.; Giri, S.; De, S.K.; Dasgupta, I.; Majumdar, S. Magnetic properties of $Ni_{2+x}Mn_{1-x}In$ Heusler alloys: Theory and experiment. *J. Magn. Magn. Mater.* **2010**, *322*, 102–107. [CrossRef]
50. Ito, W.; Xu, X.; Umetsu, R.Y.; Kanomata, T.; Ishida, K.; Kainuma, R. Concentration dependence of magnetic moment in $Ni_{50-x}Co_xMn_{50-y}Z_y$ (Z = In, Sn) Heusler alloys. *Appl. Phys. Lett.* **2010**, *97*, 242512. [CrossRef]
51. Lobo, D.N.; Priolkar, K.R.; Bhobe, P.A.; Krishnamurthy, D.; Emura, S. Correlation between local structure distortions and martensitic transformation in Ni-Mn-In alloys. *Appl. Phys. Lett.* **2010**, *96*, 232508. [CrossRef]
52. Miyamoto, T.; Ito, W.; Umetsu, R.Y.; Kainuma, R.; Kanomata, T.; Ishida, K. Phase stability and magnetic properties of $Ni_{50}Mn_{50-x}In_x$ Heusler-type alloys. *Scr. Mater.* **2010**, *62*, 151–154. [CrossRef]
53. Yin, M.; Nash, P.; Chen, W.; Chen, S. Standard enthalpies of formation of selected Ni_2YZ Heusler compounds. *J. Alloys Compd.* **2016**, *660*, 258–265. [CrossRef]
54. Brock, J.; Khan, M. Large refrigeration capacities near room temperature in $Ni_2Mn_{1-x}Cr_xIn$. *J. Magn. Magn. Mater.* **2017**, *425*, 1–5. [CrossRef]
55. Patel, A.K.; Samatham, S.S.; Suresh, K.G. Critical behavior, universality class and magneto-transport properties of Ni_2MnIn. *Mater. Res. Bull.* **2020**, *128*, 110900. [CrossRef]
56. Sakon, T.; Yamazaki, J.; Komori, T.; Kanomata, T.; Narumi, Y.; Hagiwara, M.; Nojiri, H.; Adachi, Y. The forced magnetostrictions and magnetic properties of Ni_2MnX (X = In, Sn) ferromagnetic Heusler alloys. *Materials* **2020**, *13*, 2017. [CrossRef] [PubMed]
57. Kudryavtsev, Y.V.; Lee, Y.P.; Rhee, J.Y. Dependence of the optical and magneto-optical properties and electronic structures on the atomic order in Ni_2MnIn Heusler alloys. *Phys. Rev. B* **2004**, *69*, 195104. [CrossRef]
58. Umetsu, R.Y.; Xu, X.; Ito, W.; Kainum, R. Evidence of change in the density of states during the martensitic phase transformation of Ni-Mn-In metamagnetic shape memory alloys. *Metals* **2017**, *7*, 414. [CrossRef]
59. Unzueta, I.; Sánchez-Alarcos, V.; Recarte, V.; Pérez-Landazábal, J.I.; Zabala, N.; García, J.A.; Plazaola, F. Identification of a Ni-vacancy defect in Ni-Mn-Z (Z = Ga, Sn, In): An experimental and DFT positron-annihilation study. *Phys. Rev. B* **2019**, *99*, 064108. [CrossRef]
60. Castelliz, L. Beitrag zum ferromagnetismus von legierungen der übergangsmetalle mit elementen der B-gruppe. *Z. Metallkde* **1955**, *46*, 198–203. [CrossRef]
61. Shinohara, T. Nuclear magnetic resonance in Heusler alloys: Ni_2MnSn, Co_2MnSn and Ni_2MnSb. *J. Phys. Soc. Jpn.* **1970**, *28*, 313–317. [CrossRef]
62. Leiper, W.; Geldart, D.J.W.; Pothier, P.J. Hyperfine field at the tin sites in the Heusler alloy Ni_2MnSn. *Phys. Rev. B* **1971**, *3*, 1637–1641. [CrossRef]
63. Szytuła, A.; Kołodziejczyk, A.; Rżany, H.; Todorović, J.; Wanic, A. Atomic and magnetic structure of the Heusler alloys Ni_2MnSb, Ni_2MnSn, and Co_2MnSn. *Phys. Stat. Sol. (a)* **1972**, *10*, 57–65. [CrossRef]
64. Brooks, J.S.; Williams, J.M. A Mössbauer determination of the magnitude and sign of hyperfine fields at ^{119}Sn nuclei in Heusler alloys. *J. Phys. F Metal. Phys.* **1974**, *4*, 2033–2049. [CrossRef]
65. Campbell, C.C.M.; Stager, C.V. Magnetization studies of the Heusler alloys, $Ni_2Mn_xTi_{1-x}Sn$, $Ni_2Mn_xV_{1-x}Sn$, and $Ni_2Mn_xCr_{1-x}Sn$. *Can. J. Phys.* **1976**, *54*, 2197–2203. [CrossRef]
66. MacDonald, R.A.; Stager, C.V. Magnetic properties of $(Ni_xCu_{1-x})_2MnSn$. *Can. J. Phys.* **1977**, *55*, 1481–1484. [CrossRef]

67. Sobczak, R. Magnetische Messungen an Heusler-phasen $(Co,Ni)_2XY$ (X = Ti, Zr, Hf, V und Mn; Y = Ge und Sn). *Monatsh Chem.* **1978**, *109*, 455–459. [CrossRef]
68. Hurd, C.M.; Shiozaki, I.; McAlister, S.P. On the extraordinary Hall effect in some ferromagnetic Heusler alloys. *Physica* **1981**, *107B*, 497–498. [CrossRef]
69. Kaneko, T.; Yoshida, H.; Abe, S.; Kamigaki, K. Pressure effect on the Curie point of the Heusler alloys Ni_2MnSn and Ni_2MnSb. *J. Appl. Phys.* **1981**, *52*, 2046–2048. [CrossRef]
70. Murakami, Y.; Watanabe, Y.; Kanaizuka, T.; Kachi, S. Magnetic properties and phase change of $Ni_{3-y}Mn_ySn$ alloy. *Trans. Jap. Inst. Metal* **1981**, *22*, 551–557. [CrossRef]
71. Ogiba, F.; Schreiner, W.H.; Kunzler, J.V.; Brandão, D.E. Electrical resistivity of the Ni_2MnSn Heusler alloy. *Phys. Stat. Sol. (a)* **1981**, *66*, K83–K86. [CrossRef]
72. Sobczak, R. Magnetic properties of Heusler alloys $Ni_{3-x}Mn_xSn$. *J. Magn. Magn. Mater.* **1981**, *24*, 325–327. [CrossRef]
73. Mayo, W.R.; Dunlap, R.A. Sn magnetic hyperfine field crossover in the Heusler alloys $(Ni_{1-x}Pd_x)_2MnSn$. *J. Appl. Phys.* **1982**, *53*, 8082–8084. [CrossRef]
74. Uhl, E. Magnetism in mixed Heusler alloys $(Ni_{1-x}Cu_x)_2MnSn$. *Monatsh Chem.* **1982**, *113*, 275–284. [CrossRef]
75. van Engen, P.G.; Buschow, K.H.J.; Erman, M. Magnetic properties and magneto-optical spectroscopy of Heusler alloys based on transition metals and Sn. *J. Magn. Magn. Mater.* **1983**, *30*, 374–382. [CrossRef]
76. Wachtel, E.; Henninger, F.; Predel, B. Constitution and magnetic properties of Ni-Mn-Sn alloys—Solid and liquid state. *J. Magn. Magn. Mater.* **1983**, *38*, 305–315. [CrossRef]
77. Buschow, K.H.J.; van Engen, P.G.; de Mooij, D.B. Magnetic and magneto-optical properties of Heusler alloys of the type $Ni_{3-x}Mn_xSn$. *J. Magn. Magn. Mater.* **1984**, *40*, 339–347. [CrossRef]
78. Fraga, G.L.; Kunzler, J.V.; Brandão, D.E. Spin-disorder resistivity in $Ni_2Mn(Sn_{1-x}In_x)$ Heusler alloys. *J Phys. Chem. Solids* **1985**, *46*, 1071–1075. [CrossRef]
79. Helmholdt, R.B.; Buschow, K.H.J. Crystallographic and magnetic structure of Ni_2MnSn and $NiMn_2Sn$. *J. Less-Common Metals* **1987**, *128*, 167–171. [CrossRef]
80. Gavriliuk, A.G.; Stepanov, G.N.; Sidorov, V.A.; Irkaev, S.M. Hyperfine magnetic fields and Curie temperature in the Heusler alloy Ni_2MnSn at high pressure. *J. Appl. Phys.* **1996**, *79*, 2609–2612. [CrossRef]
81. Gavriliuk, A.G.; Stepanov, G.N.; Sidorov, V.A.; Irkaev, S.M. Hyperfine magnetic fields at ^{119}Sn nuclei and Curie temperature in Heusler alloy Ni_2MnSn under high pressure. In *High Pressure Science & Technology*; Trzeciakowski, W.A., Ed.; World Scientific: Singapore, 1996; pp. 739–741.
82. Kyuji, S.; Endo, S.; Kanomata, T.; Ono, F. Pressure dependence of the Curie temperature in Ni_2MnSn Heusler alloy. *Physica B* **1997**, *237–238*, 523–524. [CrossRef]
83. Podgornykh, S.M.; Kazantsev, V.A.; Shreder, E.I. Thermal expansion of Heusler alloys NiMnSb, CuMnSb, Ni_2MnSb, and Ni_2MnSn. *Phys. Metal. Metallogr.* **1998**, *86*, 464–471.
84. Krenke, T.; Acet, M.; Wassermann, E.F.; Moya, X.; Mañosa, L.; Planes, A. Martensitic transitions and the nature of ferromagnetism in the austenitic and martensitic states of Ni-Mn-Sn alloys. *Phys. Rev. B* **2005**, *72*, 014412. [CrossRef]
85. Podgornykh, S.M.; Streltsov, S.V.; Kazantsev, V.A.; Shreder, E.I. Heat capacity of Heusler alloys: Ferromagnetic Ni_2MnSb, Ni_2MnSn, NiMnSb and antiferromagnetic CuMnSb. *J. Magn. Magn. Mater.* **2007**, *311*, 530–534. [CrossRef]
86. Kanomata, T.; Fukushima, K.; Nishihara, H.; Kainuma, R.; Ito, W.; Oikawa, K.; Ishida, K.; Neumann, K.-U.; Ziebeck, K.R.A. Magnetic and crystallographic properties of shape memory alloys $Ni_2Mn_{1+x}Sn_{1-x}$. *Mater. Sci. Forum* **2008**, *583*, 119–129. [CrossRef]
87. Chieda, Y.; Kanomata, T.; Fukushima, K.; Matsubayashi, K.; Uwatoko, Y.; Kainuma, R.; Oikawa, K.; Ishida, K.; Obara, K.; Shishido, T. Magnetic properties of Mn-rich Ni_2MnSn Heusler alloys under pressure. *J. Alloys Compd.* **2009**, *486*, 51–54. [CrossRef]
88. Kanomata, T.; Kyuji, S.; Nashima, O.; Ono, F.; Kaneko, T.; Endo, S. The Curie temperature in Heusler alloys Ni_2MnZ (Z = Ga, Sn and Sb) under high pressure. *J. Alloys Compd.* **2012**, *518*, 19–21. [CrossRef]
89. Mukadam, M.D.; Yusuf, S.M.; Bhatt, P. Tuning the magnetocaloric properties of the $Ni_{2+x}Mn_{1-x}Sn$ Heusler alloys. *J. Appl. Phys.* **2013**, *113*, 173911. [CrossRef]
90. Fichtner, T.; Kreiner, G.; Chadov, S.; Fecher, G.H.; Schnelle, W.; Hoser, A.; Felser, C. Magnetic and transport properties in the Heusler series $Ni_{2-x}Mn_{1+x}Sn$ affected by chemical disorder. *Intermetallics* **2015**, *57*, 101–112. [CrossRef]
91. Kaštil, J.; Kamarád, J.; Isnard, O.; Skourski, Y.; Míšek, M.; Arnold, Z. Effect of pressure and high magnetic field on phase transitions and magnetic properties of $Ni_{1.92}Mn_{1.56}Sn_{0.52}$ and Ni_2MnSn Heusler compounds. *J. Alloys Compd.* **2015**, *650*, 248–255. [CrossRef]
92. Nazmunnahar, M.; Ryba, T.; del Val, J.J.; Ipatov, M.; González, J.; Hošková, V.; Szabó, P.; Samuely, P.; Kravcak, J.; Vargova, Z.; et al. Half-metallic Ni_2MnSn Heusler alloy prepared by rapid quenching. *J. Magn. Magn. Mater.* **2015**, *386*, 98–101. [CrossRef]
93. Webster, P.J.; Mankikar, R.M. Chemical order and magnetic properties of the $Ni_{2-x}MnSb$ system. *J. Magn. Magn. Mater.* **1984**, *42*, 300–308. [CrossRef]

94. Khan, M.; Dubenko, I.; Stadler, S.; Ali, N. Magnetostructural phase transitions in $Ni_{50}Mn_{25+x}Sb_{25-x}$ Heusler alloys. *J. Phys. Condens. Matter* **2008**, *20*, 235204. [CrossRef] [PubMed]
95. Aksoy, S.; Acet, M.; Wassermann, E.F.; Krenke, T.; Moya, X.; Mañosa, L.; Planes, A.; Deen, P.P. Structural properties and magnetic interactions in martensitic Ni-Mn-Sb alloys. *Philo. Mag.* **2009**, *89*, 2093–2109. [CrossRef]
96. Yoshimine, Y.; Mitsunaga, D.; Orihashi, H.; Shimada, D.; Hiroi, M.; Onodera, R.; Kimura, S.; Takahashi, K.; Koyama, K. Magnetic and electrical properties of $Mn_{2-x}Ni_{1+x}Sb$. *IEEE Trans. Magn.* **2014**, *50*, 1001204.
97. Ak, F.; Öz, E.; Saatçi, B. Structural and magnetic properties of $Ni_{2-x}Co_xMnSb$ (x: 0.00, 0.25, 0.50 and 1.00) Heusler alloys: The relationship between Curie temperature and lattice parameter. *Intermetallics* **2019**, *111*, 106491. [CrossRef]
98. Ao, W.-Q.; Yu, H.-Z.; Liu, F.-L.; Liu, F.-S.; Li, J.-Q.; Du, Y.; Liu, S.-H.; Shi, C.-Y. Isothermal section of the Ni-Mn-Sb ternary system at 773 K. *J. Min. Metall. Sect. B-Metall.* **2019**, *55B*, 147–156. [CrossRef]
99. Tian, F.; Zhao, Q.; Guo, J.; Zhang, Y.; Chang, T.; Zhang, R.; Adil, M.; Zhou, C.; Cao, K.; Yang, S. The spin glass and zero-field cooling exchange bias effect observed above the curie temperature in Ni_2MnSb polycrystalline Heusler alloy. *Scr. Mater.* **2024**, *245*, 116055. [CrossRef]
100. Tian, F.; Zhao, Q.; Guo, J.; Zhang, Y.; Fang, M.; Chang, T.; Dai, Z.; Zhou, C.; Cao, K.; Yang, S. Griffiths phase arising from local lattice distortion and spin glass above the Curie temperature in Ni_2MnSb polycrystalline Heusler alloy. *Phys. Rev. B* **2024**, *109*, 224405. [CrossRef]
101. Kamarád, J.; Kaštil, J.; Friák, M.; Mazalová, M.; Schneeweiss, O.; Arnold, Z. Effect of hydrostatic pressure on magneto-crystalline anisotropy of Heusler Ni_2MnSn-based alloy. *High Press. Res.* **2021**, *41*, 405–413. [CrossRef]
102. López-García, J.; Khanna, D.L.R.; Sanchez Llamazares, J.L.; Álvarez-Alonso, P.; La Roca, P.; Recarte, V.; Sánchez-Alarcos, V.; Pérez-Landazábal, J.I.; Rodríguez-Velamazán, J.A. Magnetic structure analysis of the $L2_1$-type austenite in Ni-Mn-In alloys. *Intermetallics* **2024**, *168*, 108242. [CrossRef]
103. Noda, Y.; Ishikawa, Y. Spin waves in Heusler alloys Pd_2MnSn and Ni_2MnSn. *J. Phys. Soc. Jpn.* **1976**, *40*, 690–698. [CrossRef]
104. Bażela-Wróbel, W.; Szytuła, A. Neutron diffraction study of the $Ni_2Mn_{1-x}Cr_xSn$ system. *Phys. Stat. Sol. (a)* **1983**, *76*, K117–K120. [CrossRef]
105. Imada, S.; Yamasaki, A.; Kanomata, T.; Muro, T.; Sekiyama, A.; Suga, S. Composition dependence of Ni magnetic moment in Ni-Mn-based Heusler-type intermetallic compounds. *J. Magn. Magn. Mater.* **2007**, *310*, 1857–1858. [CrossRef]
106. Ahuja, B.L.; Dashora, A.; Heda, N.L.; Priolkar, K.R.; Vadkhiya, L.; Itou, M.; Lobo, N.; Sakurai, Y.; Chakrabarti, A.; Singh, S.; et al. Temperature dependent spin momentum densities in Ni-Mn-In alloys. *J. Phys.: Condens. Matter* **2010**, *22*, 446001. [CrossRef]
107. Mund, H.S.; Dashora, A.; Sahariya, J.; Bhamu, K.C.; Priolkar, K.R.; Lobo, N.; Itou, M.; Sakurai, Y.; Ahuja, B.L. Electronic structure and magnetic properties of Ni_2MnSn Heusler alloy. *AIP Conf. Proc.* **2011**, *1349*, 1123–1124.
108. Priolkar, K.R.; Bhobe, P.A.; Lobo, D.N.; D'Souza, S.W.; Barman, S.R.; Chakrabarti, A.; Emura, S. Antiferromagnetic exchange interactions in the $Ni_2Mn_{1.4}In_{0.6}$ ferromagnetic Heusler alloy. *Phys. Rev. B* **2013**, *87*, 144412. [CrossRef]
109. Priolkar, K.R. Role of local disorder in martensitic and magnetic interactions in Ni-Mn based ferromagnetic shape memory alloys. *Phys. Status Solidi B* **2014**, *251*, 2088–2096. [CrossRef]
110. Deb, A.; Hiraoka, N.; Itou, M.; Sakurai, Y.; Onodera, M.; Sakai, N. Spin-dependent electron momentum density in the Ni_2MnSn Heusler alloy. *Phys. Rev. B* **2001**, *63*, 205115. [CrossRef]
111. da Silva, E.Z.; Jepsen, O.; Andersen, O.K. Electronic properties of Ni-based Heusler alloys. *Solid State Commun.* **1988**, *67*, 13–14. [CrossRef]
112. Kilian, K.A.; Victora, R.H. Electronic structure of Ni_2MnIn for use in spin injection. *J. Appl. Phys.* **2000**, *87*, 7064–7066. [CrossRef]
113. Godlevsky, V.V.; Rabe, K.M. Soft tetragonal distortions in ferromagnetic Ni_2MnGa and related materials from first principles. *Phys. Rev. B* **2001**, *63*, 134407. [CrossRef]
114. Şaşıoğlu, E.; Sandratskii, L.M.; Bruno, P. First-principles calculation of the intersublattice exchange interactions and Curie temperatures of the full Heusler alloys Ni_2MnX (X = Ga, In, Sn, Sb). *Phys. Rev. B* **2004**, *70*, 024427. [CrossRef]
115. Zayak, A.T.; Entel, P.; Rabe, K.M.; Adeagbo, W.A.; Acet, M. Anomalous vibrational effects in nonmagnetic and magnetic Heusler alloys. *Phys. Rev. B* **2005**, *72*, 054113. [CrossRef]
116. Entel, P.; Buchelnikov, V.D.; Khovailo, V.V.; Zayak, A.T.; Adeagbo, W.A.; Gruner, M.E.; Herper, H.C.; Wassermann, E.F. Modelling the phase diagram of magnetic shape memory Heusler alloys. *J. Phys. D Appl. Phys.* **2006**, *39*, 865–889. [CrossRef]
117. Kurtulus, Y.; Gilleβen, M.; Dronskowski, R. Electronic structure, chemical bonding, and finite-temperature magnetic properties of full Heusler alloys. *J. Comput. Chem.* **2006**, *27*, 90–102. [CrossRef]
118. Yablonskikh, M.V.; Braun, J.; Kuchel, M.T.; Postnikov, A.V.; Denlinger, J.D.; Shreder, E.I.; Yarmoshenko, Y.M.; Neumann, M.; Moewes, A. X-ray 2*p* photoelectron and L_α resonant x-ray emission spectra of the 3*d* metals in Ni_2MnZ (Z = In, Sn, Sb) Heusler alloys. *Phys. Rev. B* **2006**, *74*, 085103. [CrossRef]
119. Zayak, A.T.; Adeagbo, W.A.; Entel, P.; Rabe, K.M. e/a dependence of the lattice instability of cubic Heusler alloys from first principles. *Appl. Phys. Lett.* **2006**, *88*, 111903. [CrossRef]

120. Pugaczowa-Michalska, M. Comparative study of compressibility of Ni_2MnX (X = In, Sn, Sb) Heusler alloys. *Acta Phys. Pol. A* **2008**, *113*, 629–632. [CrossRef]
121. Rached, H.; Rached, D.; Khenata, R.; Reshak, A.H.; Rabah, M. First-principles calculations of structural, elastic and electronic properties of Ni_2MnZ (Z = Al, Ga and In) Heulaer alloys. *Phys. Stat. Solidi B* **2009**, *246*, 1580–1586. [CrossRef]
122. Ağduk, S.; Gökoğlu, G. First-principles study of elastic and vibrational properties of Ni_2MnIn magnetic shape memory alloys. *Eur. Phys. J. B* **2011**, *79*, 509–514. [CrossRef]
123. Bai, J.; Xu, N.; Raulot, J.-M.; Zhang, Y.D.; Esling, C.; Zhao, X.; Zuo, L. First-principles investigations of crystallographic, magnetic, and electronic structures in Ni_2XIn (X = Mn, Fe, and Co). *J. Appl. Phys.* **2012**, *112*, 114901. [CrossRef]
124. Bai, J.; Xu, N.; Raulot, J.-M.; Zhang, Y.D.; Esling, C.; Zhao, X.; Zuo, L. Defect formation energy and magnetic properties of off-stoichiometric Ni-Mn-In alloys by first-principles calculations. *J. Appl. Phys.* **2013**, *113*, 174901. [CrossRef]
125. Li, C.M.; Luo, H.B.; Hu, Q.M.; Yang, R.; Johansson, B.; Vitos, L. Role of magnetic and atomic ordering in the martensitic transformation of Ni-Mn-In from a first-principles study. *Phys. Rev. B* **2012**, *86*, 214205. [CrossRef]
126. Tan, C.L.; Huang, Y.W.; Tian, X.H.; Jiang, J.X.; Cai, W. Origin of magnetic properties and martensitic transformation of Ni-Mn-In magnetic shape memory alloys. *Appl. Phys. Lett.* **2012**, *100*, 132402. [CrossRef]
127. Wang, W.; Gao, S.-S.; Meng, Y. First-principle investigations of the magnetic properties and possible martensitic transformation in Ni_2MnX (X = Al, Ga, In, Si, Ge and Sn). *J. Magn. Magn. Mater.* **2014**, *371*, 135–138. [CrossRef]
128. Borgohain, P.; Sahariah, M.B. Effect of compositional and antisite disorder on the electronic and magnetic properties of Ni-Mn-In Heusler alloy. *J. Phys. Condens. Matter* **2015**, *27*, 175502. [CrossRef] [PubMed]
129. D'Souza, S.W.; Chakrabarti, A.; Barman, S.R. Magnetic interactions and electronic structure of Ni-Mn-In. *J. Electron Spectrosc. Relat. Phenom.* **2016**, *208*, 33–39. [CrossRef]
130. Buchelnikov, V.D.; Zagrebin, M.A.; Sokolovskiy, V.V. Magnetic states of Ni_2MnZ and Ni_2CrZ (Z = Al, As, Bi, Ga, Ge, In, P, Pb, Sb, Si, Sn, Tl) Heusler alloys. *J. Magn. Magn. Mater.* **2018**, *459*, 78–83. [CrossRef]
131. Ishida, S.; Kubo, Y.; Ishida, J.; Asano, S. Electronic structures of the ferromagnetic Heusler alloys. *J. Phys. Soc. Jpn.* **1980**, *48*, 814–821. [CrossRef]
132. Kübler, J.; Williams, A.R.; Sommers, C.B. Formation and coupling of magnetic moments in Heusler alloys. *Phys. Rev. B* **1983**, *28*, 1745–1755. [CrossRef]
133. Ishida, S.; Asano, S.; Ishida, J. Bandstructures and hyperfine fields of Heusler alloys. *J. Phys. Soc. Jpn.* **1984**, *53*, 2718–2725. [CrossRef]
134. Ayuela, A.; Enkovaara, J.; Ullakko, K.; Nieminen, R.M. Structural properties of magnetic Heusler alloys. *J. Phys. Condens. Matter* **1999**, *11*, 2017–2026. [CrossRef]
135. Kurtulus, Y.; Dronskowski, R.; Samolyuk, G.D.; Antropov, V.P. Electronic structure and magnetic exchange coupling in ferromagnetic full Heusler alloys. *Phys. Rev. B* **2005**, *71*, 014425. [CrossRef]
136. Şaşıoğlu, E.; Sandratskii, L.M.; Bruno, P. Pressure dependence of the Curie temperature in Ni_2MnSn Heusler alloy: A first-principles study. *Phys. Rev. B* **2005**, *71*, 214412. [CrossRef]
137. Kulkova, S.E.; Eremeev, S.V.; Kakeshita, T.; Kulkov, S.S.; Rudenski, G.E. The electronic structure and magnetic prperties of full- and half-Heusler alloys. *Mater. Trans.* **2006**, *47*, 599–606. [CrossRef]
138. Ağduk, S.; Gökoğlu, G. Ab initio lattice dynamics of Ni_2MnX (X = Sn, Sb) magnetic shape memory alloys. *J. Alloys Compd.* **2012**, *511*, 9–13. [CrossRef]
139. Li, J.; Zhang, Z.; Sun, Y.; Zhang, J.; Zhou, G.; Luo, H.; Liu, G. The thermodynamic, electronic and magnetic properties of Ni_2MnX (X = Ge, Sn, Sb) Heusler alloys: A quasi-hormonic Debye model and first principles study. *Phys. B* **2013**, *409*, 35–41. [CrossRef]
140. Wang, X.; Shang, J.X.; Wang, F.H.; Jiang, C.B.; Xu, H.B. The structural stability and magnetic properties of the ferromagnetic Heusler alloy Ni-Mn-Sn: A first principle investigation. *J. Magn. Magn. Mater.* **2014**, *355*, 173–179. [CrossRef]
141. Hamri, B.; Abbar, B.; Hamri, A.; Baraka, O.; Hallouche, A.; Zaoui, A. Electronic structure and mechanical properties of X_2MnSn (X = Cu, Ni, Pd) under hydrostatic pressure: GGA+U calculations. *Comp. Condens. Mater* **2015**, *3*, 14–20. [CrossRef]
142. Jezierski, A. Electronic structure, magnetic, optical and thermodynamic properties of $Ni_2Mn_{1-x}Re_xSn$ and $NiMn_{1-x}Re_xSn$ Heusler alloys—Ab-initio study. *J. Alloys Compd.* **2019**, *803*, 153–164. [CrossRef]
143. Benguerine, O.; Nabi, Z.; Benichou, B.; Bouabdallah, B.; Bouchenafa, H.; Maachou, M.; Ahuja, R. Structural, elastic, electronic, and magnetic properties of Ni_2MnSb, Ni_2MnSn, and $Ni_2MnSb_{0.5}Sn_{0.5}$ magnetic shape memory alloys. *Rev. Mex. Fis.* **2020**, *66*, 121–126. [CrossRef]
144. Fischer, G.; Zubizarreta, X.; Marmodoro, A.; Hoffmann, M.; Buczek, P.; Buczek, N.; Däne, M.; Hergert, W.; Şaşıoğlu, E.; Galanakis, I.; et al. Effect of correlation and disorder on the spin-wave spectra of Pd_2MnSn, Ni_2MnSn, and Cu_2MnAl Heusler alloys: A first-principles study. *Phys. Rev. Mater.* **2020**, *4*, 064405. [CrossRef]
145. Friák, M.; Mazalová, M.; Turek, I.; Zemanová, A.; Kaštil, J.; Kamarád, J.; Míšek, M.; Arnold, Z.; Schneeweiss, O.; Všianská, M.; et al. An ab initio study of pressure-induced changes of magnetism in austenitic stoichiometric Ni_2MnSn. *Materials* **2021**, *14*, 523. [CrossRef] [PubMed]

146. Şaşıoğlu, E.; Sandratskii, L.M.; Bruno, P. Magnetic exchange coupling and Curie temperature of $Ni_{(1+x)}MnSb$ (x= 0, 0.25, 0.5, 0.75, 1) from first principles. *J. Magn. Magn. Mater.* **2005**, *290–291*, 385–387. [CrossRef]
147. Rusz, J.; Bergqvist, L.; Kudrnovský, J.; Turek, I. Exchange interactions and Curie temperatures in $Ni_{2-x}MnSb$ alloys: First-principles study. *Phys. Rev. B* **2006**, *73*, 214412. [CrossRef]
148. Rusz, J.; Kudrnovský, J.; Turek, I. Exchange interactions and correlations in $Ni_{1+x}MnSb$ Heusler alloys. *J. Magn. Magn. Mater.* **2007**, *310*, 1654–1656. [CrossRef]
149. Thoene, J.; Chadov, S.; Fecher, G.; Felser, C.; Kübler, J. Exchange energies, Curie temperatures and magnons in Heusler compounds. *J. Phys. D Appl. Phys.* **2009**, *42*, 084013. [CrossRef]
150. Ishida, S.; Asato, H.; Iwashima, E.; Kubo, Y.; Ishida, J. Fermi surfaces of Cu_2MnAl, Pd_2MnSn and Ni_2MnSn. *J. Phys. F Metal Phys.* **1981**, *11*, 1035–1046. [CrossRef]
151. Plogmann, S.; Schlathölter, T.; Braun, J.; Neumann, M.; Yarmoshenko, Y.M.; Yablonskikh, M.V.; Shreder, E.I.; Kurmaev, E.Z.; Wrona, A.; Ślebarski, A. Local moments in Mn-based Heusler alloys and their electronic structures. *Phys. Rev. B* **1999**, *60*, 6428–6438. [CrossRef]
152. Jezierski, A.; Kowalewski, P.; Dubowik, J. Role of the magnetic impurities in $Ni_2Ti_{1-x}Mn_xSn$ Heusler type alloys. Ab-initio calculations. *Mater. Sci.-Poland* **2007**, *25*, 553–557.
153. Kulkova, S.; Eremeev, S.; Hu, Q.M.; Li, C.M.; Yang, R. The influence of defects and composition on the electronic structure and magnetic properties of shape memory Heusler alloys. *ESOMAT* **2009**, *2009*, 02017.
154. Bose, S.K.; Kudrnovský, J.; Drchal, V.; Turek, I. Magnetism of mixed quaternary alloys: (Ni, T)$_2$MnSn (T = Cu,Pd) as a case study. *Phys. Rev. B* **2010**, *82*, 174402. [CrossRef]
155. Rauf, S.; Arif, S.; Haneef, M.; Amin, B. The first principle study of magnetic properties of Mn_2WSn, Fe_2YSn (Y = Ti, V), Co_2YSn (T = Ti, Zr, Hf, V, Mn) and Ni_2YSn (Y = Ti, Zr, Hf, V, Mn) heusler alloys. *J. Phys. Chem. Solids* **2015**, *76*, 153–169. [CrossRef]
156. Roy, T.; Pandey, D.; Chakrabarti, A. Probing the possibility of coexistence of martensite transition and half-metallicity in Ni and Co-based full-Heusler alloys: An *ab initio* calculation. *Phys. Rev. B* **2016**, *93*, 184102. [CrossRef]
157. Govind, B.; Bharti, P.; Srivastava, M.; Kumar, A.; Bano, S.; Bhatt, K.; Tawale, J.S.; Pulikkotil, J.J.; Misra, D.K. Magnetic properties of intermediate $Ni_{2-x}Mn_{1+x}Sb$ full-Heusler compounds. *Mater. Res. Bull.* **2021**, *142*, 111427. [CrossRef]
158. Li, Y.; Bai, J.; Sun, S.; Jin, M.; Zhang, Y.; Liang, X.; Cu, J.; Zhang, Y.; Esling, C.; Zhao, X.; et al. Composition-dependent phase transformation path involving 4O martensite in Ni-Mn-Sn magnetic shape memory alloys. *J. Appl. Phys.* **2022**, *132*, 135110. [CrossRef]
159. Bose, S.K.; Kudrnovský, J.; Drchal, V.; Turek, I. Pressure dependence of Curie temperature and resistivity in complex Heusler alloys. *Phys. Rev. B* **2011**, *84*, 174422. [CrossRef]
160. Buchelnikov, V.D.; Sokolovskiy, V.V. Magnetocaloric effect in Ni-Mn-X (X = Ga, In, Sn, Sb) Heusler alloys. *Phys. Met. Metallogr.* **2011**, *112*, 633–665. [CrossRef]
161. Buchelnikov, V.D.; Sokolovskiy, V.V.; Taskaev, S.V.; Khovaylo, V.V.; Aliev, A.A.; Khanov, L.N.; Batdalov, A.B.; Entel, P.; Miki, H.; Takagi, T. Monte Carlo simulations of the magnetocaloric effect in magnetic Ni-Mn-X (X = Ga, In) Heusler alloys. *J. Phys. D Appl. Phys.* **2011**, *44*, 064012. [CrossRef]
162. Siewert, M.; Gruner, M.E.; Hucht, A.; Herper, H.C.; Dannenberg, A.; Chakrabarti, A.; Singh, N.; Arróyave, R.; Entel, P. A first-principles investigation of the compositional dependent properties of magnetic shape memory Heusler alloys. *Adv. Eng. Mater* **2012**, *14*, 530–546. [CrossRef]
163. Sokolovskiy, V.V.; Buchelnikov, V.D.; Zagrebin, M.A.; Entel, P.; Sahool, S.; Ogura, M. First-principles investigation of chemical and structural disorder in magnetic $Ni_2Mn_{1+x}Sn_{1-x}$ Heusler alloys. *Phys. Rev. B* **2012**, *86*, 134418. [CrossRef]
164. Ishikawa, Y.; Noda, Y. Spin waves and magnetic interactions in the ferromagnetic Heusler alloys. *AIP Conf. Proc.* **1975**, *24*, 145–151.
165. Robey, S.W.; Hudson, L.T.; Kurtz, R.L. Resonant-photoemission investigation of the Heusler alloys Ni_2MnSb and NiMnSb. *Phys. Rev. B* **1992**, *46*, 11697–11704. [CrossRef]
166. Kimura, A.; Suga, S.; Shishidou, T.; Imada, S.; Muro, T.; Park, S.Y.; Miyahara, T.; Kaneko, T.; Kanomata, T. Magnetic circular dichroism in the soft-x-ray absorption spectra of Mn-based magnetic intermetallic compounds. *Phys. Rev. B* **1997**, *56*, 6021–6030. [CrossRef]
167. Imada, S.; Yamasaki, A.; Kusuda, K.; Higashiya, A.; Irizawa, A.; Sekiyama, A.; Kanomata, T.; Suga, S. Ultraviolet photoemission of Ni_2MnZ (Z = Ga, In and Sn). *J. Electron Spectrosc. Relat. Phenom.* **2007**, *156–158*, 433–435. [CrossRef]
168. Ye, M.; Kimura, A.; Miura, Y.; Shirai, M.; Cui, Y.T.; Shimada, K.; Namatame, H.; Taniguchi, M.; Ueda, S.; Kobayashi, K.; et al. Role of electronic structure in the martensitic phase transition of $Ni_2Mn_{1+x}Sn_{1-x}$ studied by hard-x-ray photoelectron spectroscopy and *ab initio* calculation. *Phys. Rev. Lett.* **2010**, *104*, 176401. [CrossRef] [PubMed]
169. Zhu, S.; Ye, M.; Shirai, K.; Taniguchi, M.; Ueda, S.; Miura, Y.; Shirai, M.; Umetsu, R.Y.; Kainuma, R.; Kanomata, T.; et al. Drastic change in density of states upon martensitic phase transition for metamagnetic shape memory alloy $Ni_2Mn_{1+x}In_{1-x}$. *J. Phys. Condens. Matter* **2015**, *27*, 362201. [CrossRef] [PubMed]
170. Kuz'min, R.N.; Ibraimov, N.S.; Zhdanov, G.S. Mössbauer effect in Heusler alloys. *Sov. Phys. JETP* **1966**, *23*, 219–224.

171. Geldart, D.J.W.; Campbell, C.C.M.; Pothier, P.J.; Leiper, W. Mössbauer effect study of the hyperfine fields at the tin sites in Cu_2MnSn, Ni_2MnSn, and Pd_2MnSn. *Can. J. Phys.* **1972**, *50*, 206–212. [CrossRef]
172. Love, J.C.; Obenshain, F.E. Hyperfine fields at Ni sites in Heusler alloys. *AIP Conf. Proceed.* **1972**, *5*, 538.
173. Swartzendruber, L.J.; Evans, B.J. Hyperfine fields at the antimony sites in the Heusler-type Ni_xMnSb alloys. *AIP Conf. Proceed.* **1972**, *5*, 539–543.
174. Campbell, C.C.M. Hyperfine field systematics in Heusler alloys. *J. Phys. F Metal Phys.* **1975**, *5*, 1931–1945. [CrossRef]
175. Williams, J.M.; Danson, D.P. A Mössbauer study of the Heusler alloy series $Ni_2Mn_xTi_{1-x}Sn$. *J. Phys. Colloque* **1979**, *40*, C2–C169. [CrossRef]
176. Birchall, T.; Ruebenbauer, K.; Campbell, C.C.M. Magnetic ordering in the Heusler alloys $Ni_2Mn_xY_{1-x}Sn$ (Y = Ti, V) studied by ^{119}Sn Mössbauer spectroscopy. *Phys. Stat. Solidi (a)* **1980**, *57*, 381–392. [CrossRef]
177. Dunlap, R.A.; March, R.H.; Stroink, G. Sn hyperfine field distributions in the Heusler alloys XMnSn and X_2MnSn. *Can. J. Phys.* **1981**, *59*, 1577–1584. [CrossRef]
178. Delyagin, N.N.; Krylov, V.I.; Nesterov, V.I. Magnetic hyperfine interaction of ^{119}Sn impurity atoms in ordered alloys of iron with palladium and platinum. Radial dependence of the partial contributions to the magnetic hyperfine field. *Sov. Phys. JETP* **1980**, *52*, 532–538.
179. Friák, M.; Schneeweiss, O.; Kamarád, J.; Kaštil, J.; Miroshkina, O.N.; Gruner, M.E. Impact of swaps on Mössbauer characteristics of Ni_2MnSn: An experimental and quantum-mechanical study. *J. Mater. Sci.* **2024**, *59*, 5595–5606. [CrossRef]
180. Le Dang, K.; Veillet, P.; Campbell, I.A. Hyperfine fields at sp sites in Heusler alloys. *J. Phys. F Metal. Phys.* **1977**, *7*, 2561–2566.
181. Le Dang, K.; Veillet, P.; Campbell, I.A. Magnetic interactions and conduction electron polarization studied by NMR in Heusler alloys. *J. Phys. F Metal Phys.* **1977**, *7*, L237–L241.
182. Le Dang, K.; Veillet, P.; Campbell, I.A. Hyperfine fields and magnetic interactions in Heusler alloys. *J. Phys. F Metal Phys.* **1978**, *8*, 1811–1825.
183. Schaf, J.; Le Dang, K.; Veillet, P.; Campbell, I.A. Extended and local effects of cold work in Heusler alloys. *J. Phys. F Metal Phys.* **1983**, *13*, 1311–1316. [CrossRef]
184. Elfazani, M.; DeMarco, M.; Jha, S.; Julian, G.M.; Blue, J.W. Hyperfine magnetic field at cadmium impurity in Heusler alloys Ni_2MnGa, Ni_2MnIn, Cu_2MnIn, and Au_2MnIn. *J. Appl. Phys.* **1981**, *52*, 2043–2045. [CrossRef]
185. Hamzić, A.; Asomoza, R.; Campbell, I.A. The transport properties of Heusler alloys: 'ideal' local moment ferromagnets. *J. Phys. F Metal Phys.* **1981**, *11*, 1441–1447. [CrossRef]
186. McAlister, S.P.; Shiozaki, I.; Hurd, C.M.; Stager, C.V. Galvanomagnetic effects in the Ni_2MnSn Heusler alloy. *J. Phys. F Metal Phys.* **1981**, *11*, 2129–2138. [CrossRef]
187. Kudrnovský, J.; Drchal, V.; Turek, I.; Khmelevskyi, S.; Glasbrenner, J.K.; Belashchenko, K.D. Spin-disorder resistivity of ferromagnetic metals from first principles: The disordered-local-moment approach. *Phys. Rev. B* **2012**, *86*, 144423. [CrossRef]
188. Miroshkina, O.N.; Eggert, B.; Lill, J.; Beckmann, B.; Koch, D.; Hu, M.Y.; Lojewski, T.; Rauls, S.; Scheibel, F.; Taubel, A.; et al. Impact of magnetic and antisite disorder on the vibrational densities of states in Ni_2MnSn Heusler alloys. *Phys. Rev. B* **2022**, *106*, 214302. [CrossRef]
189. Kokorin, V.V.; Osipenko, I.A.; Shirina, T.V. Phase transitions in alloys $Ni_2MnGa_xIn_{1-x}$. *Phys. Met. Metallogr.* **1989**, *67*, 173–176.
190. Kanomata, T.; Kaneko, T. *Magnetic Properties of d-Elements, Alloys and Compounds Under Pressure*; Kawazoe, Y., Kaneko, T., Uwatoko, Y., Eds.; Landort-Börnstein, New Series, Group IV/22A; Springer: Berlin-Heidelberg, Germany, 2014.
191. Lázpita, P.; L'vov, V.A.; Rodríguez Fernández, J.; Barandiarán, J.M.; Chernenko, V.A. Combined effect of magnetic field and hydrostatic pressure on the phase transitions exhibited by Ni-Mn-In metamagnetic shape memory alloy. *Acta Mater.* **2020**, *193*, 1–9. [CrossRef]
192. Rungger, I.; Sanvito, S. *Ab initio* study of the magnetostructural properties of MnAs. *Phys. Rev. B* **2006**, *74*, 024429. [CrossRef]
193. Khovaylo, V.V.; Kanomata, T.; Tanaka, T.; Nakashima, M.; Amako, Y.; Kainuma, R.; Umetsu, R.Y.; Morito, H.; Miki, H. Magnetic properties of $Ni_{50}Mn_{34.8}In_{15.2}$ probed by Mössbauer spectroscopy. *Phys. Rev. B* **2009**, *80*, 144409. [CrossRef]
194. Forrer, R. Distances magnétiques efficaces dans les métaux, alliages et combinaisons ferromagnétiques et antiferromagnétiques du groupe du fer. *Ann. Phys.* **1952**, *12*, 605–621. [CrossRef]
195. Seshu Bai, V.; Rajasekharan, T. Evidence of a critical Mn-Mn distance for the onset of ferromagnetism in NiAs type compounds. *J. Magn. Magn. Mater.* **1984**, *42*, 198–200. [CrossRef]
196. Yamada, N. Atomic magnetic moment and exchange interaction between Mn atoms in intermetallic compounds in Mn-Ge system. *J. Phys. Soc. Jpn.* **1990**, *59*, 273–288. [CrossRef]
197. Bose, S.K.; Kudrnovský, J.; Drchal, V. Magnetism and electronic transport in $(Ni,Cu)_2MnSn$ Heusler alloys under ambient and elevated pressures. *World J. Eng.* **2012**, *9*, 13–21. [CrossRef]
198. Williams, K.; Cagin, T. Anisotropic elastic properties of Ni-Mn-In magnetic shape memory alloy. *ICCES* **2010**, *15*, 153–160.
199. Qawasmeh, Y.; Hamad, B. Investigation of the structural, electronic, and magnetic properties of Ni-based Heusler alloys from first principles. *J. Appl. Phys.* **2012**, *111*, 033905. [CrossRef]

200. Li, C.M.; Hu, Q.M.; Yang, R.; Johansson, B.; Vitos, L. Magnetic ordering and physical stability of $X_2Mn_{1+x}Sn_{1-x}$ (X = Ru, Os, Co, Rh, Ni, Pd, Cu, and Ag) Heusler alloys from a frst-principles study. *Phys. Rev. B* **2013**, *88*, 014109. [CrossRef]
201. Peng, W.; Zhang, D.H.; Xu, N. Bulk modulus and thermodynamic properties of $L2_1$ Ni_2XY (X = Mn, Fe, Co, Y = Ga, In) compounds studied by first-principles calculations. *J. Mater. Sci.* **2017**, *52*, 1149–1155. [CrossRef]
202. Yan, H.L.; Liu, H.X.; Zhang, M.J.; Jia, N.; Bai, J.; Yang, B.; Li, Z.; Zhang, Y.; Esling, C.; Zhao, X.; et al. Electronic origin of the main-group element dependences of elastic moduli in the Ni_2Mn-based magnetic shape memory alloys. *J. Phys. Chem. Solids* **2021**, *148*, 109671. [CrossRef]
203. Moriya, T.; Kawabata, A. Effect of spin fluctuations on itinerant ferromagnetism. *J. Phys. Soc. Jpn.* **1973**, *34*, 639–651. [CrossRef]
204. Moriya, T. *Spin Fluctuations in Itinerant Electron Magnetism*; Springer: Berlin Heidelberg, Germany, 1985.
205. Takahashi, Y. On the origin of the Curie-Weiss law of the magnetic susceptibility in itinerant electron ferromagnetism. *J. Phys. Soc. Jpn.* **1986**, *55*, 3553–3573. [CrossRef]
206. Takahashi, Y. *Spin Fluctuation Theory of Itinerant Electron Magnetism*; Springer: Berlin Heidelberg, Germany, 2013.
207. Ziebeck, K.R.A.; Capellmann, H.; Brown, P.J.; Booth, J.G. Spin fluctuations in both the ordered and paramagnetic phases of MnSi! MnSi a heavy Fermi liquid? *Z. Phys.B* **1982**, *48*, 241–250. [CrossRef]
208. Nishihara, H.; Komiyama, K.; Oguro, I.; Kanomata, T.; Chernenko, V. Magnetization processes near the Curie temperatures of the itinerant ferromagnets, Ni_2MnGa and pure nickel. *J. Alloys Compd.* **2007**, *442*, 191–193. [CrossRef]
209. Sakon, T.; Hayashi, Y.; Fujimoto, N.; Kanomata, T.; Nojiri, H.; Adachi, Y. Forced magnetostriction of ferromagnetic Heusler alloy Ni_2MnGa at the Curie temperature. *J. Appl. Phys.* **2018**, *123*, 213902. [CrossRef]
210. Sakon, T.; Hayashi, Y.; Li, D.; Honda, F.; Oomi, G.; Narumi, Y.; Hagiwara, M.; Kanomata, T.; Eto, T. Forced magnetostrictions and magnetizations of $Ni_{2+x}MnGa_{1-x}$ at its Curie temperature. *Materials* **2018**, *11*, 2115. [CrossRef] [PubMed]
211. Sakon, T.; Hayashi, Y.; Fukuya, A.; Li, D.; Honda, F.; Umetsu, R.Y.; Xu, X.; Oomi, G.; Kanomata, T.; Eto, T. Investigation of the itinerant electron feromagnetism of $Ni_{2+x}MnGa_{1-x}$ and Co_2VGa Heusler alloys. *Materials* **2019**, *12*, 575. [CrossRef] [PubMed]
212. Kanomata, T.; Nishihara, H.; Osaki, T.; Doi, M.; Sakon, T.; Adachi, Y.; Kihara, T.; Obara, K.; Shishido, T. Magnetic properties of ferromagnetic Heusler alloy Co_2NbGa. *J. Magn. Magn. Mater.* **2020**, *503*, 166604. [CrossRef]
213. Yoshinaga, S.; Mitsui, Y.; Umetsu, R.Y.; Koyama, K. Magnetic properties of Cr-based ternary compound CrAlGe. *Phys. Procedia* **2015**, *75*, 918–925. [CrossRef]
214. Tateiwa, N.; Pospíšil, J.; Haga, Y.; Sakai, H.; Matsuda, T.D.; Yamamoto, E. Itinerant ferromagnetism in actinide 5 f –electron systems: Phenomenological analysis with spin fluctuation theory. *Phys. Rev. B* **2017**, *96*, 035125. [CrossRef]
215. Opletal, P.; Valenta, J.; Proschek, P.; Sechovský, V.; Prokleška, J. Effect of localization of 5f-electrons and pressure on magnetism in uranium intermetallics in spin-fluctuation theory. *Phys. Rev. B* **2020**, *102*, 094409. [CrossRef]
216. Faske, T.; Radulov, I.A.; Hölzel, M.; Gutfleisch, O.; Donner, W. Direct observation of paramagnetic spin fluctuations in $LaFe_{13-x}Si_x$. *J. Phys. Condens. Matter.* **2020**, *32*, 115802. [CrossRef] [PubMed]
217. Wohlfarth, E.P. Metallic magnetism under high pressure. In *Physics of Solids under High Pressure*; Schilling, J.S., Shelton, R.N., Eds.; North-Holland Pub. Co.: Amsterdam, The Netherlands, 1981; pp. 175–180.
218. Yoshinaga, S.; Miura, S.; Kanomata, T.; Mitsui, Y.; Koyama, K. Pressure effect on magnetism of weak itinerant electron ferromagnet $Ni_{74.6}Al_{25.4}$. *IEEE Magn. Lett.* **2017**, *8*, 1400403. [CrossRef]
219. Buis, N.; Franse, J.J.M.; Brommer, P.E. The magnetic properties of Ni_3Al under high pressures. *Physica* **1981**, *106B*, 1–8. [CrossRef]
220. Huber, J.G.; Maple, M.B.; Wohlleben, D.; Knapp, G.S. Magnetic properties of $ZrZn_2$ under pressure. *Solid State Commun.* **1975**, *16*, 211–216. [CrossRef]
221. Beille, J.; Bloch, D.; Towfiq, F. High pressure magnetic properties of $Fe_xCo_{1-x}Ti$ alloys. *Solid State Commun.* **1978**, *25*, 57–59. [CrossRef]
222. Beille, J.; Bloch, D.; Towfiq, F.; Voiron, J. The magnetic properties of $Fe_xCo_{1-x}Si$ and $Fe_xCo_{1-x}Ti$ alloys. *J. Magn. Magn. Mater.* **1979**, *10*, 265–273. [CrossRef]
223. Patrick, L. The change of ferromagnetic Curie points with hydrostatic pressure. *Phys. Rev.* **1954**, *93*, 384–392. [CrossRef]
224. Kondorskii, E.I.; Sedov, V.L. The change of atomic magnetic moments in ferromagnetic metals under hydrostatic compression. *Sov. Phys. JETP* **1960**, *11*, 561–565.
225. Shigeta, I.; Fujimoto, Y.; Ooka, R.; Nishisako, Y.; Tsujikawa, M.; Umetsu, R.Y.; Nomura, A.; Yubuta, K.; Miura, Y.; Kanomata, T.; et al. Pressure effect on the magnetic properties of the half-metallic Heusler alloy Co_2TiSn. *Phys. Rev. B* **2018**, *97*, 104414. [CrossRef]
226. Adachi, Y.; Ogi, Y.; Osaki, T.; Eto, T.; Kihara, T.; Nishihara, H.; Sakon, T.; Gouchi, J.; Uwatoko, Y.; Kanomata, T. Pressure effect on the magnetic properties of the Heusler alloy Co_2NbGa. *J. Supercond. Nov. Magn.* **2024**, *37*, 249–254. [CrossRef]
227. Tedrow, P.M.; Meservey, R. Spin polarization of electrons tunneling from films of Fe, Co, Ni, and Gd. *Phys. Rev. B* **1973**, *7*, 318–326. [CrossRef]

Disclaimer/Publisher's Note: The statements, opinions and data contained in all publications are solely those of the individual author(s) and contributor(s) and not of MDPI and/or the editor(s). MDPI and/or the editor(s) disclaim responsibility for any injury to people or property resulting from any ideas, methods, instructions or products referred to in the content.